

The RGB Sample of Intermediate BL Lacs

S. A. Laurent-Muehleisen

(slauren@igpp.llnl.gov)

University of California-Davis and

The Institute for Geophysics and Planetary Physics,

Lawrence Livermore National Laboratory

7000 East Ave., Livermore, CA 94550, USA

R. I. Kollgaard

(rik@fnal.gov)

Fermi National Accelerator Laboratory, Batavia, IL 60510, USA

E. D. Feigelson

(edf@astro.psu.edu)

Dept. of Astro. & Astrophys., The Pennsylvania State University,

University Park, PA 16802, USA

W. Brinkmann and J. Siebert

(wpb@rzg.mpg.de, jos@mpe.mpg.de)

Max-Planck-Institut für extraterrestrische Physik,

Giessenbachstrasse, D-85740, Garching, Germany

ABSTRACT

Combining newly identified and previously known BL Lacs from the RASS-Green Bank (RGB) catalog, we present a sample of 127 BL Lacs, the largest ever derived from a single uniform survey. A Complete sample of 33 objects brighter than $O=18.0$ mag is also presented. These samples are compared to other known BL Lac samples and are generally found to exhibit properties intermediate between those of the previously disparate classes of High and Low energy peaked BL Lacs (HBLs and LBLs, respectively). This result is most dramatic in the distribution of the X-ray to radio logarithmic flux ratios, where the RGB BL Lacs are shown to peak precisely where the sharp dichotomy between the two subclasses was previously seen. The α_{ro} vs. α_{ox} diagram also shows the RGB sample smoothly bridges the gap between the previously distinct subclasses of LBLs and HBLs. The range of broadband Spectral Energy Distributions (SEDs) exhibited by the RGB objects also shows that contrary to prior claims, searches based on relatively deep surveys cannot limit followup spectroscopy to targets with a narrow range of SEDs since BL Lacs clearly constitute a homogeneous population with a wide range of SEDs.

Similar to results based on the EMSS and 1Jy BL Lac samples, we find a weak, but statistically significant correlation between the composite X-ray spectral index α_{xox}

and the radio-optical spectral index α_{ro} . This implies that the more LBL-like RGB BL Lacs have a secondary source of X-ray emission, possibly from an inverse Compton component. This result, in addition to other characteristics of the RGB sample, indicates that the simple unified scheme which postulates HBLs and LBLs differ solely by orientation may be in need of revision. We also present both the X-ray and radio $\log N - \log S$ distributions for which the competing HBL/LBL unification scenarios have differing predictions. The unknown effects of the triple flux limit inherent in the RGB Complete sample makes quantitative analysis uncertain, but the characteristics of the RGB sample compare well both with results obtained from previous samples and with general theoretical predictions based on a simple Monte Carlo simulation. Our analysis indicates that the unimodal distribution of BL Lac properties found in the RGB sample likely reliably reflect the underlying population, while the bimodal distribution found in earlier studies arose primarily from observational selection effects. The presence of not only intermediate, but also extreme HBL and LBL objects is the RGB survey’s unique strength and offers clear avenues for future studies which can undoubtedly address the question of how HBLs and LBLs are related.

Subject headings: BL Lacertae objects: general — galaxies: active — radio continuum: galaxies — surveys — X-ray: general

1. Introduction

BL Lacs comprise a rare subclass of Active Galactic Nuclei (AGN) and are characterized by a lack of prominent emission lines, a highly variable nonthermal continuum and strong, variable optical polarization (Kollgaard 1994; Urry and Padovani 1995). Additional characteristics include the lack of a UV-excess (or “blue bump”) and a core-dominated radio morphology (Angel and Stockman 1980; Wardle et al. 1984; Laurent-Muehleisen et al. 1993). The dominance of nonthermal radiation at all wavelengths ranging from the radio to gamma ray regimes is well-established (Sambruna et al. 1996, and references therein) and makes BL Lacs particularly interesting laboratories for the study of AGN phenomena.

Numerous studies have shown that BL Lacs contain relativistic jets which produce narrow cones of beamed emission which makes the observed radiation sensitive to orientation of the jet axis relative to the line-of-sight (see Kollgaard 1994; Urry and Padovani 1995, and references therein). BL Lacs are associated with those objects that are oriented such that their jets lie close to the line-of-sight while the parent population of misaligned objects are postulated to be low luminosity Fanaroff-Riley Type I radio galaxies (Fanaroff and Riley 1974; Browne 1983). This association between BL Lacs and FR I galaxies is one of the stronger links in the “unified scheme” of AGN where observed properties are primarily a result of orientation rather than intrinsic astrophysical differences (e.g., Antonucci 1993).

However, it has not been clear whether all BL Lac properties can be attributed to orientation differences, nor whether BL Lacs constitute a homogeneous class. For example, the broadband spectral energy distributions (SEDs) of BL Lacs discovered in X-ray and radio surveys differ significantly which has led to the subclassification of BL Lacs into X-ray-selected and radio-selected objects (XBLs and RBLs, respectively). This has recently been supplanted by a new classification “High energy peaked BL Lacs” (HBLs) and “Low energy peaked BL Lacs” (LBLs) based on the ratio of X-ray to radio flux densities, S_x/S_r (Giommi and Padovani 1994; Padovani and Giommi 1995a). Generally, XBLs tend to be HBLs and exhibit less extreme properties than RBLs which are usually LBLs.

The two BL Lac subclasses exhibit systematically distinct properties, including the degree of radio core dominance, optical polarization fraction and duty cycle, fraction of optical host galaxy light, and perhaps even parsec-scale jet speeds, megaparsec-scale clustering properties and host galaxy optical and radio luminosities (Laurent-Muehleisen et al. 1993; Perlman and Stocke 1993; Jannuzzi et al. 1994; Wurtz et al. 1996; Kollgaard et al. 1996a, 1999). Many of these characteristics are consistent with the unified scheme paradigm if HBLs are objects which lie further from the line-of-sight than LBLs. However, orientation by itself cannot explain the apparent lack of BL Lacs with properties intermediate between the LBL and HBL subclasses.

There is also increasing concern that the simplest unified scheme may not account for all subclass distinctions. Intrinsic as well as orientation differences may be present. For example, estimates of jet speeds and angles to the line-of-sight of HBLs, LBLs and FR I radio galaxies

do not appear to be able to account for all differences in the SEDs (Sambruna et al. 1996). In addition, estimates of space densities are inconsistent with orientation values, and the cosmic evolution of the classes appears to be incompatible (Rector et al. 1999a).

These issues have proved difficult to address because existing BL Lac samples are still relatively small and were generated from shallow surveys which contain only the very brightest objects in either the radio or X-ray wavebands. These and other selection effects have produced samples biased towards the most extreme HBLs or LBLs with few transitional objects. The sample of BL Lacs presented here was generated from a cross-correlation of a deep radio (Laurent-Muehleisen et al. 1997) and X-ray catalog and contains BL Lacs with the full range of properties from HBLs to LBLs. This RASS-Green Bank (RGB) BL Lac sample is the largest BL Lac sample yet created from a uniformly defined set of criteria. It consists of 127 objects drawn from a correlation of the ROSAT All-Sky Survey (RASS) and a reanalysis of the 1987 Green Bank 6 cm radio survey (GB96, Gregory et al. 1996). The design and followup spectroscopic observations of this sample are presented in Laurent-Muehleisen et al. (1998, hereafter Paper I). Here we concentrate specifically on the RGB BL Lacs and on what they reveal about the relationship between the BL Lac subclasses.

This paper is organized as follows. In §2 we briefly review the RASS/GB correlation and our followup VLA and optical observations. The RGB and “RGB Complete” samples are presented in §3 and §4. Sections 5 and 6 analyze these samples’ bulk characteristics and discuss their astrophysical implications. We assume throughout $H_0=100 \text{ km s}^{-1} \text{ Mpc}^{-1}$, $q_0=0.5$ and define spectral indices, α , such that $S_\nu \propto \nu^{-\alpha}$.

2. Selection of Candidate Objects

Both radio and X-ray surveys have proven to be a rich source of new BL Lacs. The largest purely radio-selected sample is that based on the 1 Jy survey while the most prominent X-ray-selected samples are those based on the Einstein Extended Medium Sensitivity Survey (EMSS; Gioia et al. 1990; Stocke et al. 1991; Maccacaro et al. 1994) and the HEAO-1 Large Area Sky Survey (Wood et al. 1984; Kollgaard et al. 1996b). As the flux limit and/or sky coverage of radio and X-ray surveys has improved and the ability to fully identify all objects in these surveys has become impractical, the technique of selecting candidate BL Lacs based on the broadband SEDs of previously known BL Lacs has proven to be highly efficient. The Einstein Slew Survey (Elvis et al. 1992; Schachter et al. 1993a; Perlman et al. 1996a), Hamburg Quasar Survey (Hagen et al. 1995; Nass et al. 1996), Deep X-ray Radio Blazar Survey samples (Perlman et al. 1998) and the optical polarization sample of Kock et al. (1996) were all created by spectroscopically classifying sources with counterparts detected concurrently in the more than one band. Nevertheless, the number of objects in each of these samples has remained relatively small and their selection effects are often difficult to assess (see, e.g., Browne and Marchā 1993). The need for a large sample with a minimal number of simple selection criteria is clear.

The potential of the ROSAT All-Sky Survey for creating just such a BL Lac sample has been noted (Stocke et al. 1989) and followup programs are confirming this prediction. Some programs based on the RASS have used the optical polarization or narrowly defined broadband SEDs to select BL Lac candidates (Kock et al. 1996; Nass et al. 1996). These candidates were chosen independent of any knowledge of the radio flux of the source, but followup observations have shown that all are detected at centimeter wavelengths (Nass et al. 1996), a result in agreement with the assertion that radio-silent BL Lacs are very rare or possibly nonexistent (Stocke et al. 1990). Our RGB BL Lac sample was therefore constructed using previously detected radio emission as a criterion. This sample is therefore triply flux-limited (radio, optical and X-ray) but imposes no other selection criteria other than location in the northern hemisphere ($0^\circ < \delta < 75^\circ$; Laurent-Muehleisen et al. 1997). This method coupled with high sensitivity of the RGB survey in these three wavebands detects BL Lacs with a variety of broadband SEDs.

The initial RGB catalog consisted of sources whose positions differed by less than $100''$ in the RASS and a point source catalog created from the 1987 Green Bank 6 cm radio survey (GB96, Gregory et al. 1996; Neumann et al. 1994). This new GB catalog consists of 3σ and greater confidence sources and has a flux density limit of ~ 15 mJy in the declination range from $30^\circ - 75^\circ$ and increases to ~ 24 mJy at low declinations (Neumann et al. 1994). In order to eliminate spurious RASS-GB coincidences and to determine positions accurate enough for reliable optical identification, the 2,127 sources in the RASS-GB correlation were observed at high resolution with the NRAO's¹ VLA. Two radio catalogs were produced, the first consists of 1,861 sources for which subarcsecond positions and core radio flux densities were obtained; the second consists of 436 sources for which only low resolution data ($\sim 8''$ positional accuracy) were obtained (Laurent-Muehleisen et al. 1997). Our analysis showed that all sources whose radio and X-ray positions differed by less than $40''$ are true matches to a high degree of confidence. Additional details on the RASS-GB correlation and the followup radio observations can be found in Laurent-Muehleisen et al. (1997) and Laurent-Muehleisen (1996)².

Optical counterparts were determined via Automatic Plate Measuring scans of the high Galactic latitude ($> 25^\circ$) POSSI photographic plates (Kibblewhite et al. 1984). Optical counterparts within $3''$ of RGB sources were identified and both the O (blue) and E (red) magnitudes measured (Laurent-Muehleisen 1996; Brinkmann et al. 1997). A looser criterion of $5''$ was used for sources in the low resolution VLA catalog. Spectra were obtained for 169 optically bright ($O \leq 18.5$ mag) objects which lacked spectroscopic classifications (Paper I).

Table 1 summarizes the steps involved in the creation of the final RGB catalog. A discussion of the broadband multiwavelength properties of the entire RGB sample can be found in Paper I and Brinkmann et al. (1997) as well as Laurent-Muehleisen (1996).

¹NRAO is operated by Associated Universities, Inc., under cooperative agreement with the National Science Foundation.

²This Ph.D. thesis is available via the WWW at <http://www-igpp.llnl.gov/people/slauren.html>

TABLE 1
RGB CATALOG CREATION SUMMARY

Step	# of Sources	Notes
Initial RASS-GB Correlation	2,127	Match Criterion: $\Delta_{R/X} = 100''$
Followup VLA Radio Sources	2,297	Some GB sources became >1 VLA source 1,861 from high radio resolution data 436 from low radio resolution data 83 Empty fields 2 Not observed
Reliable RASS-VLA Matches	1,567	Match Criterion: $\Delta_{VLA/X} = 40''$
Reliable RASS-VLA-POSS I Matches	971	796 from high radio resolution data Match Criterion: $\Delta_{VLA/Opt} = 3''$ 175 from low radio resolution data Match Criterion: $\Delta_{VLA/Opt} = 5''$
Spectroscopically Classified Sources	594	Includes 140 new IDs from Laurent-Muehleisen et al. 1998 548 from high radio resolution data 46 from low radio resolution data
RGB BL Lacs	127	100 are unambiguous BL Lacs (27 are transitional objects) 107 IDs are from high radio resolution data

We noted in Paper I that the operational definition of a BL Lac has changed since that of Stein et al. (1976) who defined a BL Lac as an AGN having a highly variable, linearly polarized, nonthermal continuum without optical emission lines. More recently, Stocke et al. (1991) defined a BL Lac as an AGN with emission lines whose equivalent width does not exceed 5 Å and whose Ca II H&K break strength (Br_{4000}) is $\leq 25\%$ ³. However, recent observations, particularly of the less extreme HBLs, has shown that even this definition is too stringent and excludes objects which otherwise exhibit BL Lac-like properties and should therefore be classified as such (Marchā et al. 1996; Scarpa and Falomo 1997). Establishing a set of criteria which define the BL Lac class is particularly difficult because much of the observed emission is contributed by orientation-dependent beamed radiation while the creation of unbiased samples requires that the classification of objects be based on intrinsic (not observed) characteristics. In Paper I, we adopted the classification criteria proposed by Marchā et al. (1996) to distinguish BL Lacs from ordinary quasars, Seyfert, radio and elliptical galaxies. Briefly, our classification scheme is:

- If the spectrum is featureless or the only features observed are emission lines with $W_\lambda \leq 5$ Å (rest frame), the object is classified as a BL Lac.
- If absorption features are present and $Br_{4000} < 25\%$, we classify the object as a BL Lac, provided any emission lines present have $W_\lambda \leq 5$ Å.
- If the Ca II break contrast is between 25%–40%, we classify the object as a possible BL Lac if any emission line present also has an equivalent width smaller than that required by the Marchā et al. (1996) criterion for that particular break strength (see Paper I).
- If the Ca II break contrast was $> 40\%$ we classified the object as a galaxy because of the lack of spectroscopic evidence for an AGN, although we find no clear discontinuity in properties which distinguishes BL Lacs from galaxies (Paper I, Figure 3).

Our spectroscopic observations combined with these criteria produced a sample of 53 RGB BL Lacs, 38 of which were newly discovered. We now combine these objects with previously identified BL Lacs in the RGB catalog and discuss the full sample.

3. The RGB Sample of BL Lacs

The RGB sample consists of 127 sources of which 100 are definitive BL Lacs. Many of the 27 objects which are only probable BL Lacs have break contrasts larger than 25%, but adhere to the Marchā Br_{4000} – W_λ criteria. Twenty of the RGB BL Lacs belong to the low radio resolution

³The Ca II break contrast refers to the relative depression of the continuum blueward of the Ca II H&K lines (3933 Å & 3968 Å).

subset of the RGB catalog. Because core radio flux characterizes many of the beaming properties of BL Lacs, we exclude these “low radio resolution objects” from all further analysis, reducing the sample of objects we discuss to 107 RGB BL Lacs which is the largest sample of BL Lacs ever cataloged from one survey.

For completeness, all 127 sources are presented in Table 2. The columns give the (1) RGB Name; (2) alternate Name; (3) and (4) J2000 coordinates; (5) RGB 5 GHz core radio flux density (in mJy); (6) X-ray flux (in 10^{-12} erg s $^{-1}$ cm $^{-2}$ in the 0.1-2.4 keV ROSAT band); (7) O magnitude from the APM POSS-I catalog; (8) ROSAT PSPC X-ray spectral energy index; (9) and (10) the α_{ro} and α_{ox} spectral indices; (11) redshift and (12) references. As discussed in Brinkmann et al. (1997), Laurent-Muehleisen et al. (1997) and Laurent-Muehleisen et al. (1998), the uncertainties on the multiband fluxes can be taken to be approximately 20%, 0.5 mag and 25% in the radio, optical and X-ray, respectively.

Flux densities in Table 2 have not been K-corrected, but the two-point spectral indices (α_{ro} and α_{ox}) are corrected assuming a flat ($\alpha_r=0.0$) radio spectral index and an X-ray spectral index as given in column 8, or the mean X-ray spectral index of $\alpha_x=1.2$, valid for a large sample of RASS-detected BL Lacs (Brinkmann et al. 1997). When a measured redshift is unavailable, the K-correction is based on the median RGB BL Lac redshift, $z=0.16$. Although this probably underestimates these objects’ true redshift (objects with $z \leq 0.16$ would likely show spectral evidence for the host galaxy and hence would have a measured redshift), we feel it is important to apply some type of K-correction to all objects since the K-correction always produces a net flattening of the α_{ro} and α_{ox} spectral indices (given our assumptions). However, the effect is small, typically producing an error of ≤ 0.05 in either index unless the true redshift is > 1.0 .

The optical magnitudes are equivalent O band values, converted from other bands assuming $\alpha_{\text{opt}}=1.0$ when no O or B magnitudes were available in the literature. (The notes to Table 2 also give the original magnitude and band.) If any galaxy absorption features were detected, we corrected the magnitudes to include only the contribution from the AGN component using the method described in Paper I. We note that these corrections have only been made for the newly identified objects presented in Paper I because the correction requires the determination of the Ca II break contrast which is usually not reported in the literature.

The K-corrected radio–optical and optical–X-ray spectral indices are defined to be $\alpha_{\text{ro}}=0.194 \log \left(\frac{S_5^{\text{core}}}{S_{\text{opt}}} \right)$ and $\alpha_{\text{ox}}=0.351 \log \left(\frac{S_{\text{opt}}}{S_X} \right)$ and are given in columns 9 & 10. The monochromatic ROSAT X-ray flux density was converted from the fluxes given in Table 2 according to:

$$S_X = 4.138 \times 10^{-18} \cdot F_X \cdot E^{-\alpha_x} \left[\frac{1 - \alpha_x}{2.4^{(1-\alpha_x)} - 0.1^{(1-\alpha_x)}} \right] \quad (1)$$

where E is set at 2 keV, F_X is in erg s $^{-1}$ cm $^{-2}$ and S_X is in erg s $^{-1}$ cm $^{-2}$ keV $^{-1}$. The values of

α_{ro} and α_{ox} are accurate to ± 0.1 and ± 0.2 , respectively, taking into account the observational uncertainties in the fluxes. This does not, however, include the effects of real temporal variability in these nonsimultaneous multiband data. Generally speaking, variability is unlikely to change the flux values by more than 25% and the two-point spectral indices given in the table are therefore reasonably representative.

Finally we note that a few RGB sources identified as BL Lacs in the literature are missing from Table 2 and therefore technically not members of the RGB BL Lac sample. RGB J1058+564, RGB J1110+715, and RGB J1610+671B have spectra that were presented in Paper I, but violate the radio/X-ray coincidence criterion of $\Delta_{\text{rx}} \leq 40''$. The previously known BL Lacs RGB J0738+177 (PKS 0735+178) and RGB J1508+271 are respectively $3.1''$ and $3.8''$ from bright optical sources and therefore do not appear in Table 2 since they violate our radio/optical coincidence criterion. However, both are likely true RGB BL Lacs⁴.

4. The RGB Complete Sample

The RGB sample was constructed without imposing any selection criteria other than the presence of an optical counterpart within $3''$ ($5''$ for the low radio resolution sample) and a RASS source within $40''$ of a GB96 radio source. These well-defined criteria allowed us to create the “RGB Complete Sample” which consists of optically bright objects (total O magnitude < 18.0) observed over 3970 deg^2 of the sky with a completeness of 94% (Figure 1).

Our complete survey area contains a total of 183 RGB sources, most of which are emission-line AGN (68%) and galaxies (12%). But 33 are optically bright BL Lacs (including three candidate objects with Ca II break contrasts between 29-39%) which constitute the RGB Complete BL Lac Sample. These objects are listed separately in Table 2. The RGB Complete sample is therefore flux-limited in three bands: radio, optical and X-ray. The constraints imposed by the RASS survey (whose flux limit varies with ecliptic latitude and N_{H}) and the GB survey (whose flux density limit varies slightly with declination) both affect the catalog’s overall completeness but in a well-defined manner. The effects of the optical flux limit are more serious than those imposed by the X-ray and radio limits. Assuming all BL Lacs have color-color indices in the range $0.1 < \alpha_{\text{ro}} < 0.8$ and $0.5 < \alpha_{\text{ox}} < 2.1$ (see Figure 3), a limiting optical magnitude of $O = 18.0 \text{ mag}$ implies that the RGB Complete sample is only truly complete above $S_{\text{r}} = 3 \text{ Jy}$ and $F_{\text{X}} = 10^{-11} \text{ erg s}^{-1} \text{ cm}^{-2}$, criteria which are satisfied by none of the BL Lacs in this sample. However, the situation is less dire in practice since the RGB Complete sample is constructed from surveys with well-defined flux limits but without any additional selection criteria applied to it. Any additional constraints (such as limiting

⁴Source 0930+4950 is a BL Lac but was incorrectly reported in Laurent-Muehleisen et al. (1997) as belonging to the RGB catalog of X-ray and radio-emitting AGN. We therefore also exclude this object from the current paper.

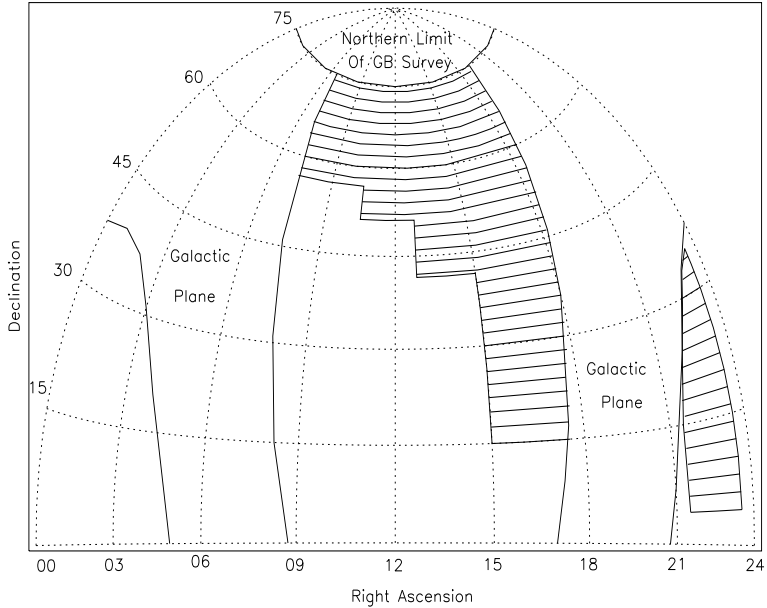


Fig. 1.— The 3970 deg^2 from which the RGB Complete sample was selected. The Galactic plane ($b < 25^\circ$) and northern extent of the GB survey ($\delta = 75^\circ$) are labeled. The region designated by the horizontal lines constitutes the RGB Complete Survey area which consists of the following six regions: (1) $6^{\text{h}}30^{\text{m}} < \alpha < 10^{\text{h}}31^{\text{m}}$ and $57^\circ 40' < \delta < 75^\circ$ (2) $10^{\text{h}}31^{\text{m}} < \alpha < 12^{\text{h}}48^{\text{m}}$ and $50^\circ < \delta < 75^\circ$ (3) $12^{\text{h}}48^{\text{m}} < \alpha < 15^{\text{h}}$ and $40^\circ 30' < \delta < 75^\circ$ (4) $15^{\text{h}} < \alpha < 19^{\text{h}}$ and $15^\circ < \delta < 75^\circ$ and (5) $21^{\text{h}}30^{\text{m}} < \alpha < 23^{\text{h}}30^{\text{m}}$ and $3^\circ < \delta < 34^\circ$ with the added constraint that $b > 25^\circ$.

candidates to objects with particular SEDs), however, would be much less useful for characterizing the full BL Lac population.

We note that three previously known BL Lacs nearly, but do not exactly, satisfy the criteria for inclusion in the RGB Complete sample. First, 1ES 2326+174 is 16.8 mag Slew Survey BL Lac with 27 mJy radio flux and $1.5 \times 10^{-11} \text{ erg s}^{-1} \text{ cm}^{-2}$ X-ray flux (Perlman et al. 1996a). This source lies in a region of the All-Sky Survey where the standard data screening software finds very little acceptable data, reducing the effective exposure time to essentially zero. This source therefore did not appear in our original RASS–GB correlation and is therefore missing from the current RGB BL Lac sample. Second, as mentioned in §3, RGB J1058+564 and RGB 1508+271 are BL Lacs that respectively violate our radio/X-ray and radio/optical offset criteria. With these possible exceptions, our 33 source optically bright RGB BL Lac sample is complete given our selection criteria and therefore constitutes a useful sample for statistical study.

5. Properties of the RGB Sample

To assess the characteristics of the RGB sample, we compare it with four large, well-defined samples of BL Lacs currently available in the literature: the 1 Jy, HEAO, EMSS and Einstein Slew Survey samples (Stickel et al. 1991; Stocke et al. 1991; Perlman et al. 1996a; Remillard et al. 1986; Schwartz et al. 1989). We will treat the RBL 1 Jy sample as representing the range of properties associated with LBLs (Low energy peaked BL Lacs), although the recent assertion that some 1 Jy objects may be misclassified microlensed sources should be noted (Stocke and Rector 1997). The XBL EMSS and HEAO samples will be combined to represent HBLs (High energy peaked BL Lacs). As will be shown below, the Slew Survey objects tend to exhibit properties intermediate between HBLs and LBLs and are in that sense similar to the RGB sample. The occasional duplication of a source in more than one sample is ignored here.

We compare the distributions of redshift, three representations of SED shape – S_x/S_r ratio, $\alpha_{xox} = \alpha_{ox} - \alpha_x$ (Sambruna et al. 1996) and location in the α_{ro} vs. α_{ox} plane – and the radio and X-ray BL Lac logN–LogS relations. Data for the comparison samples were obtained from the literature, mainly from Laurent-Muehleisen et al. (1993), Kollgaard et al. (1996b), Sambruna et al. (1996), Perlman et al. (1996a), Perlman et al. (1996b), Urry et al. (1996), Brinkmann et al. (1997) and Paper I. The median values for the various samples are given below in Table 3 and were calculated using the Astronomy SURVival analysis software (ASURV, Rev. 1.2, LaValley et al. 1992, which can be obtained from <http://www.astro.psu.edu/statcodes>) which properly handles the upper and lower limits present in the data. (One source has an upper limit to its core radio flux density, RGB J1000+225A.) Median values are calculated using the maximum-likelihood Kaplan-Meier estimator and the statistical significance of any differences between two samples is estimated with the logrank and Peto & Peto generalized Wilcoxon tests (Feigelson and Nelson 1985).

Table 3. Median Properties of BL Lac Samples

Property	HEAO	EMSS	XBL (HEAO+ EMSS)	Slew	RGB Complete	RGB	1 Jy
Redshift	0.12	0.30	0.20	0.16	0.13	0.16	0.50
$\log S_x/S_r$	-4.78	-4.84	-4.79	-4.56	-5.56	-5.61	-6.89
α_{xox}	-0.25	-0.13	-0.17	-0.23	-0.11	-0.14	0.23

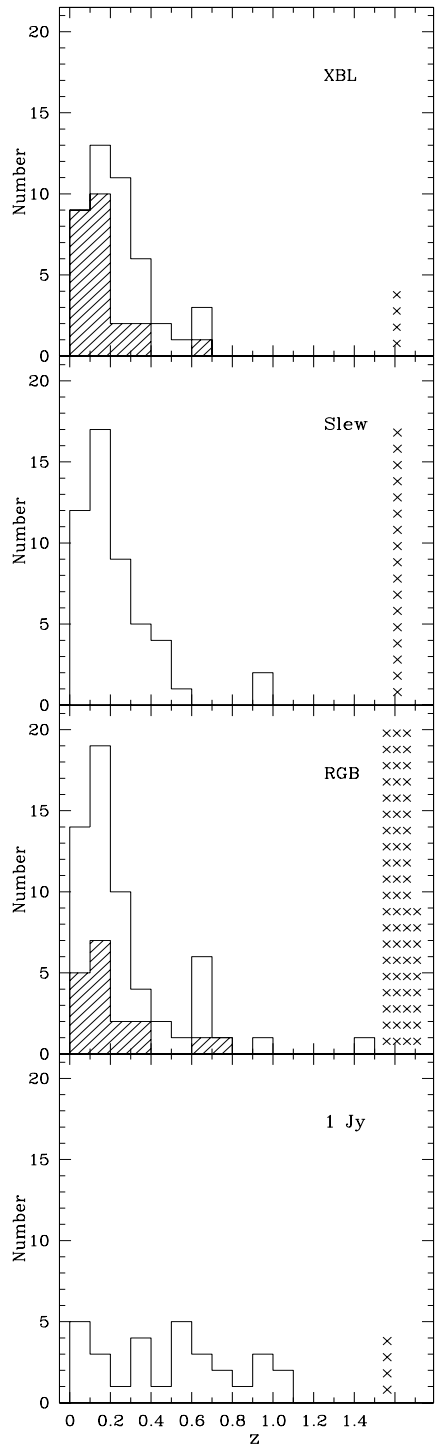


Fig. 2.— The redshift distribution for the various BL Lac samples. **a.** The XBL sample of BL Lacs which consists of both the EMSS and HEAO objects. The hatched region denotes the HEAO objects and the top solid line is the sum of both samples. **b.** The Slew survey sample of BL Lacs. **c.** The RGB sample of BL Lacs. The hatched region denotes the RGB Complete sample of bright objects. **d.** The 1 Jy sample of RBLs. The \times 's on the far right represent objects with unknown redshifts.

5.1. Redshift Distribution

Figure 2 shows the distribution of redshifts for the RGB sample as well as the XBL, Slew Survey, and 1 Jy samples. A typical HBL clearly resides at a lower redshift than a typical LBL, a trend which is predicted by the unified model of Fossati et al. (1997) which asserts that HBLs constitute the intrinsically lower luminosity sources. Although redshifts are known for only approximately half (59) of the RGB sources, RGB redshifts span nearly the entire range exhibited both by HBLs and LBLs but they are heavily weighted toward lower redshifts with a smaller median redshift (0.16) than most samples. The median redshift of the RGB Complete sample is essentially the same as the full RGB sample.

Not surprisingly, many of the lowest redshift objects in the RGB BL Lac sample exhibit a Ca II break contrast: 13 of the 17 RGB BL Lacs with measurable Ca II break contrasts lie below the median redshift. This implies that earlier samples which required Ca II break contrasts to be less than 25% are missing a significant fraction of low redshift objects, a result also obtained in the preliminary work on the “REX” BL Lac sample (Caccianiga et al. 1999). Perlman et al. (1996a) noted the typical redshift of a Slew Survey BL Lac is much lower than that of an EMSS object, perhaps indicating the EMSS sample is incomplete due to misclassification. Recent observations indeed show that four EMSS objects should be reclassified as BL Lacs based on the Marchā et al. (1996) criteria (Rector et al. 1999a). These points illustrate the ambiguity in the current definitions for BL Lacs. The Marchā et al. (1996) criteria, adopted in our RGB sample, are however an important step toward a standard, meaningful definition that is largely independent of orientation and encompasses the lower luminosity (and presumably more numerous) objects.

5.2. The α_{ro} vs. α_{ox} Diagram

In Figure 3 we present the α_{ro} vs. α_{ox} color-color diagram for the RGB and comparison BL Lac samples. The spectral indices for the comparison samples have been recalculated using our assumptions (§3) and based on data in the literature. When the redshift is unknown, we use the median redshift for objects in that sample (see Table 3). However, we were not able to correct the optical fluxes from other samples to include emission from only the AGN component, as we did for the RGB sample because the Ca II break contrasts are generally unavailable. The correction for host galaxy starlight is typically an increase (decrease) in α_{ro} (α_{ox}) of 0.06 (0.11) for the 17 “corrected” RGB objects which has little effect on the $\alpha_{\text{ro}}-\alpha_{\text{ox}}$ diagram. Additionally, unlike most diagrams of this type, the radio flux density used to calculate the α_{ro} spectral index includes the 5 GHz flux from only the arcsecond-scale radio core which best represents the beamed component. This is an important point, as extended emission is frequently comparable to core emission in HBLs (Laurent-Muehleisen et al. 1993; Perlman and Stocke 1993).

Figure 3 shows the RGB BL Lacs exhibit a smooth distribution in α_{ox} , ranging from 0.46–1.72, with no hint of the bimodality which has been previously widely discussed (e.g., Brinkmann et al.

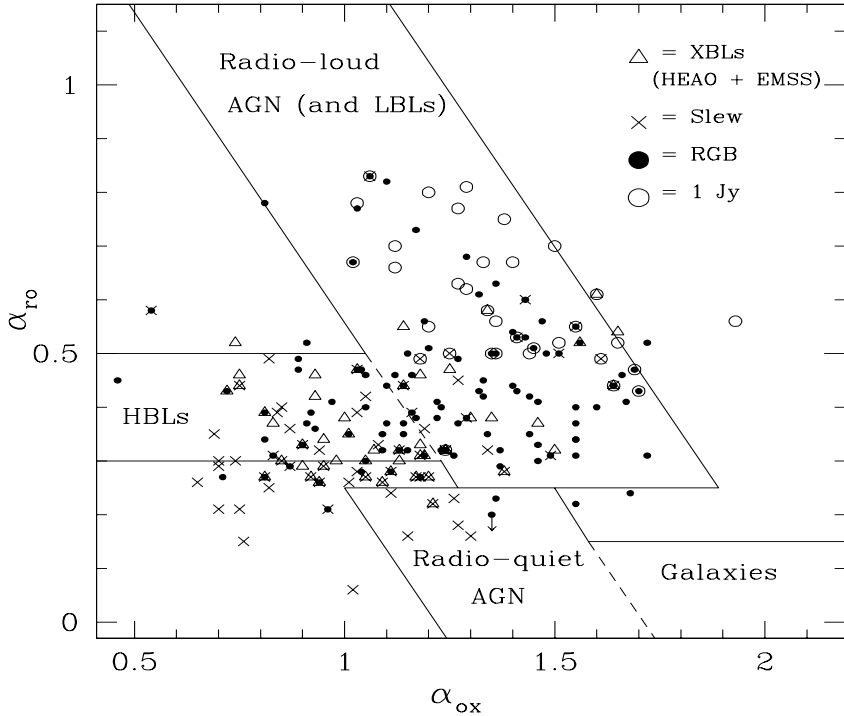


Fig. 3.— The α_{ro} vs. α_{ox} color-color diagram for various samples of BL Lacs. The flux densities used to calculate the spectral indices have all been K-corrected and converted to 5 GHz (radio core), 4400 Å, and 2 keV for the three bands. Objects common to more than one sample are plotted using the symbols representing all samples to which they belong. The EMSS-defined class boundaries are also shown for comparison. Note that the RGB sample spans both the traditional HBL region (defined by the EMSS and HEAO samples) and the LBL region (defined by the 1 Jy sample).

1996). This result is in agreement with early results from the “DXRBS” (Perlman et al. 1998) and “REX” (Caccianiga et al. 1999) samples which show that a large number of intermediate objects exists and that there is no clear separation of the HBL and LBL subclasses (see also §5.3 below). This implies the apparent bimodality could have been caused by selection effects inherent in the two best-studied, previously known samples: the EMSS and 1 Jy, a question we will examine in greater detail in §6.

Both the RGB and Slew survey objects lie in regions of flatter α_{ro} and steeper α_{ox} than the EMSS or 1 Jy BL Lacs. Generally, the RGB BL Lacs lie along a horizontal band defined by $0.2 < \alpha_{\text{ro}} < 0.6$. All but one of the RGB objects with $\alpha_{\text{ro}} > 0.6$, also have $\alpha_{\text{ox}} > 1.0$ and therefore have LBL-like SEDs, although few RGB objects appear to be as extreme as the majority of 1 Jy BL Lacs. This likely occurs because any RGB object fainter than $O \approx 18.5$ mag (the magnitude limit for most of the RGB sample) with $\alpha_{\text{ro}} \geq 0.6$ must be very radio bright, $S_r \gtrsim 200$ mJy, a flux density large enough to exclude the majority of RGB objects. In contrast, the 1 Jy sample has an

optical magnitude limit of $V \sim 20$ mag and therefore contains objects with very steep values of α_{ro} . As the identification of the RGB catalog (Laurent-Muehleisen et al. 1997) is extended to fainter optical magnitudes, we expect objects with flat α_{ox} but steep α_{ro} spectral indices (i.e., extreme LBL-like BL Lacs) will be discovered.

5.3. X-ray to Radio Flux Density Ratios

Previous BL Lac samples show a clear bimodality in the ratio of the X-ray to radio flux densities of HBLs and LBLs at $\log S_X/S_r \simeq -5.5$ (Padovani and Giommi 1995a; Perlman et al. 1996a; Brinkmann et al. 1996). In contrast, the RGB BL Lacs have a median X-ray to radio logarithmic flux density ratio of -5.61 (Table 3). The distribution of the flux ratios (Figure 4) shows no evidence for a sharp division between the two subclasses. The RGB catalog is therefore the first to contain large numbers intermediate BL Lacs, although hints that these objects existed have been previously reported by Perlman et al. (1998), Caccianiga et al. (1999) and Laurent-Muehleisen et al. (1998).

Statistical two-sample tests show that the RGB and the RGB Complete samples are consistent with having been drawn from the same distribution. This indicates that the bright optical magnitude limit imposed on the RGB Complete sample does not drastically affect the overall distribution of S_X/S_r and, by extension, the fraction of HBLs vs. LBLs, a property for which the different unification models have significantly different predictions. Studies of the properties of the Complete Sample can therefore yield important insights into the origin of the HBL vs. LBL subclasses.

5.4. High Energy Continuum: α_{xox}

The X-ray emission mechanism in both HBLs and LBLs is most likely dominated by synchrotron radiation at low energies and inverse-Compton (IC) processes at higher (γ -ray) energies (Blandford and Rees 1978; Ghisellini et al. 1985; Bregman et al. 1987). The shape of the X-ray spectrum is useful for determining at what energy this transition takes place which is important for understanding the overall energy budget and underlying jet physics in BL Lacs.

While X-ray spectral indices characterize the high energy continuum, the composite X-ray/optical spectral index, $\alpha_{xox} = \alpha_{ox} - \alpha_x$ more precisely measures changes in the SED between the optical and soft X-ray bands by distinguishing the relative importance of IC and synchrotron emission processes. If $\alpha_{xox} \leq 0$, then the X-rays lie along a powerlaw or steepening synchrotron continuum. A positive value of α_{xox} represents a concave spectrum and is likely caused by a hard IC component.

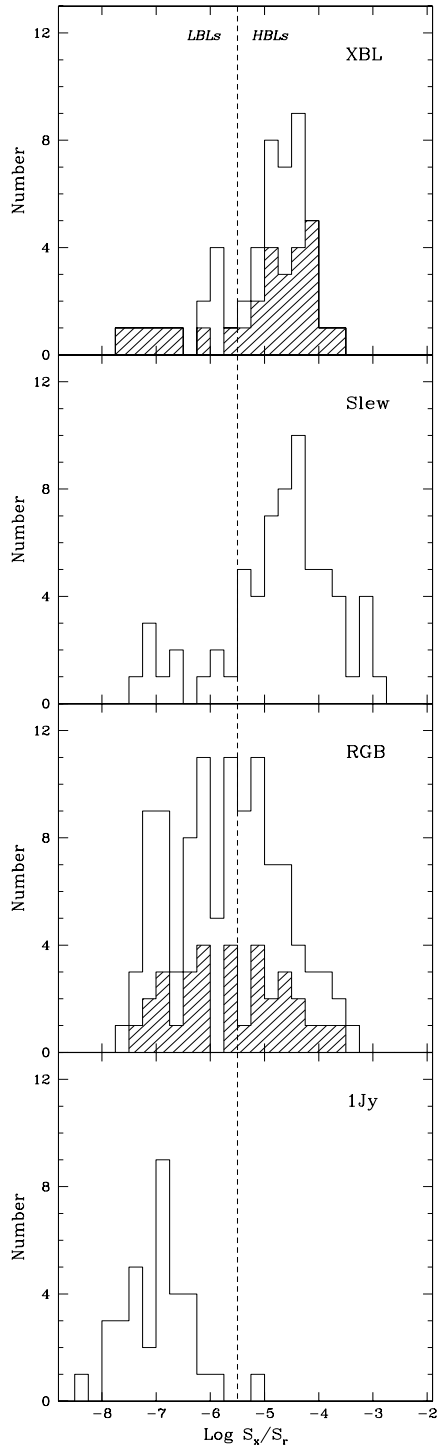


Fig. 4.— The distribution of the logarithm of the X-ray to radio flux density ratios for various samples of BL Lacs **a**. The XBL sample **b**. The Slew survey sample **c**. The RGB sample **d**. The 1 Jy sample. Hatched regions are as described in Figure 2. Unlike many other samples, we consider here only the core radio flux density. The division between HBLs and LBLs, as defined by the flux ratios of previously known samples, clearly occurs at $\log S_x/S_r = -5.5$. The RGB sample shows no such dichotomy and also includes objects with traditional HBL- and LBL-like SEDs.

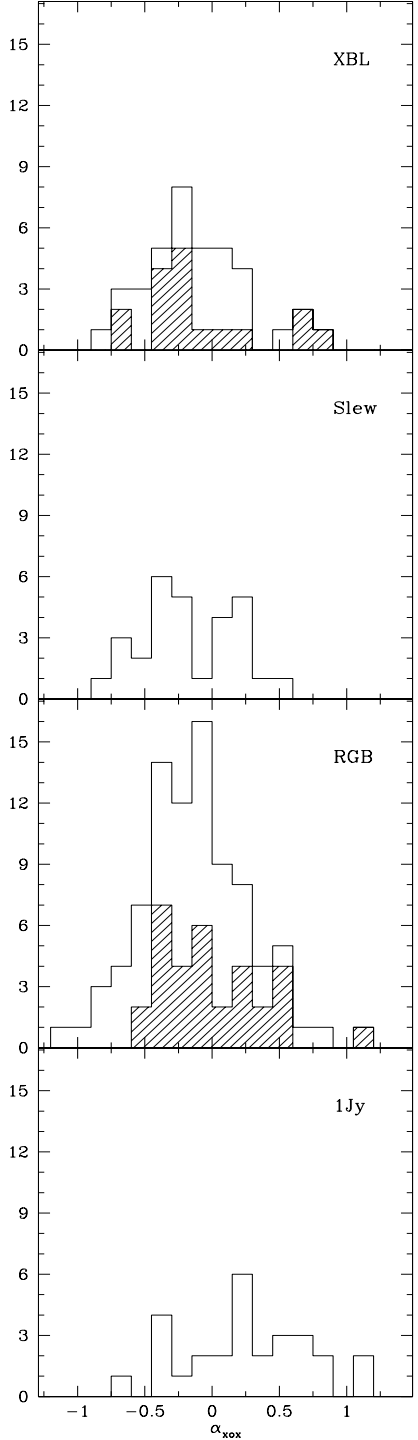


Fig. 5.— The distribution of the difference between the optical–X-ray and X-ray spectral indices, $\alpha_{\text{xox}} = \alpha_{\text{ox}} - \alpha_{\text{x}}$, for various BL Lac samples **a**. The XBL sample **b**. The Slew survey sample **c**. The RGB sample **d**. The 1 Jy sample. Hatched regions are as described in Figure 2.

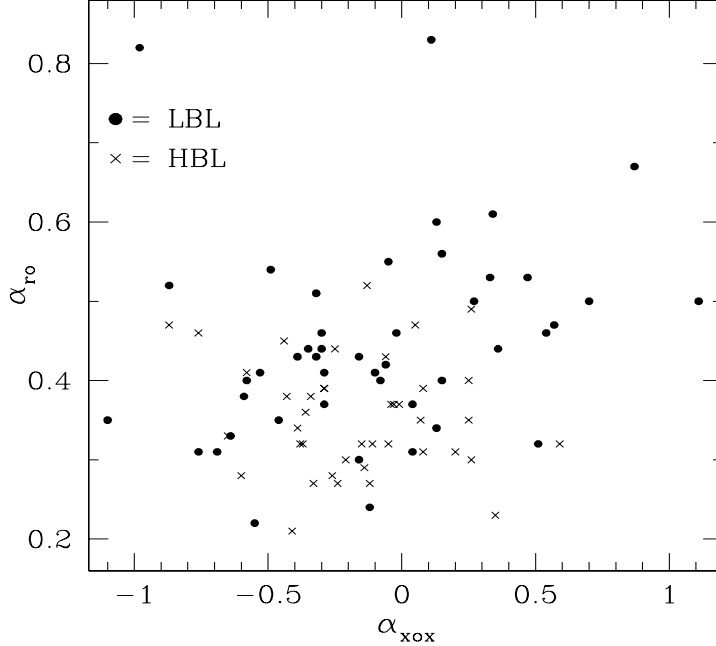


Fig. 6.— The α_{ro} vs. α_{xox} diagram for the RGB BL Lacs. Filled circles represent LBLs and X's represent HBLs. There is a weak ($P=92\%$) correlation present. Note that LBLs tend to be the objects with the steepest α_{ro} and positive (“convex”) $\alpha_{xox} = \alpha_{ox} - \alpha_x$.

If LBLs and HBLs differ solely by orientation, then it should be possible to explain differences in their SEDs by invoking beaming models and varying only one free parameter, the angle to the line-of-sight. However, Sambruna et al. (1996) find that there are differences in the SEDs of LBLs and HBLs which are not attributable to orientation alone: objects with steeper α_{ro} spectral indices (generally LBLs) have a tendency to also have more positive values of α_{xox} . This indicates the presence of a second, presumably hard IC, X-ray component and suggests there are intrinsic differences between LBLs and HBLs which are independent of orientation.

Figure 5 shows the distribution of α_{xox} for the XBL, Slew, RGB and 1 Jy samples. Only those objects with measured X-ray spectral indices are included (82% of the RGB sample). As seen for other parameters, the RGB sample spans the range exhibited by the extremes of LBLs and HBLs and many sources exhibit intermediate properties; the RGB Complete sample exhibits similar characteristics (Table 3). To test the results of Sambruna et al. (1996), we searched for a correlation between α_{ro} and α_{xox} in the RGB sample (Figure 6). Objects have been divided into HBL- and LBL-like classes based on their X-ray to radio flux ratios. There is a correlation with moderate statistical significance ($P \simeq 92\%$ using a nonparametric Spearman's ρ statistic) for the RGB BL Lacs. This is weaker than the correlation found by Sambruna et al. (1996) who found $P > 99.99\%$ using the EMSS and 1 Jy samples. However, if we supplement the intermediate RGB objects with BL Lacs from the EMSS, HEAO and 1 Jy samples, the probability that a correlation

is present increases to >99.99%. It is not surprising that the addition of the extreme HBLs (which lie in the bottom left corner of the diagram) and the extreme LBLs (which lie in the upper right corner) strengthen the correlation. This shows that the full range of high energy spectral shapes exhibited by BL Lacs does correlate with BL Lac subclass, confirming the results of Sambruna et al. (1996).

5.5. X-ray logN–logS Relationship

Both the X-ray and radio logN-logS distributions of the EMSS and 1 Jy BL Lacs have been studied extensively. However, as the results presented here show that BL Lacs do not belong to two distinct subclasses, conclusions drawn from studies of the logN-logS distribution of only the two extremes of the BL Lac population may be misleading. Nevertheless, theoretical models based on the 1 Jy and EMSS data have made interesting predictions. Based on the standard orientation-based beamed jet model unifying FRI radio galaxies and BL Lacs, the known FRI luminosity function and observational constraints on jet Lorentz factors, Urry et al. (1991) calculate the radio radio logN-logS distribution of BL Lacs down to 1 mJy. We compare the Complete RGB sample to these predictions and other BL Lac samples.

One caveat regarding the completeness of the sample bears mentioning. We characterize the RGB BL Lacs' radio emission using core flux densities which can often fall significantly below the total flux density as measured in the original Green Bank survey. As a consequence, only those objects with low radio core-to-lobe ratios populate the lowest radio flux density bins. (Faint radio sources with high radio core-to-lobe ratios will have total radio flux densities below the GB survey flux limit and will be missing from our survey.) Only the lowest radio flux density bins (<20 mJy based on the GB96 survey flux limit) are affected by this source of incompleteness.

Figure 7 shows the X-ray logN-logS distribution for the RGB Complete, EMSS and Hamburg Quasar Survey samples (HQS, Hagen et al. 1995; Nass et al. 1996). Here we truncate the EMSS and HQS samples so that they match the selection criteria present in the RGB Complete catalog, namely the objects must be brighter than $O=18.0$ mag in the optical and bright enough in the radio to be present in the GB96 catalog. This eliminates 19 of the 22 EMSS objects, while the HQS sample is diminished from 61 objects to 27.

Also shown in the figure is the Euclidean no-evolution model defined by $N(>F_X) \propto F_X^{-3/2}$ and arbitrarily normalized to $N(>F_X) = 2.0 \times 10^{-3}$ at $F_X = 1.5 \times 10^{-11} \text{ erg s}^{-1} \text{ cm}^{-2}$. All three samples fall well below the Euclidean relationship at faint flux levels. The RGB catalog exhibits a higher density of objects than the HQS given identical flux limits. At a flux of $\sim 10^{-12} \text{ erg s}^{-1} \text{ cm}^{-2}$, the HQS number density is ~ 1.7 times lower than the RGB sample likely a result of the very restrictive $\alpha_{\text{ox}} < 1.1$ ($\log(S_X/S_o) > 1.3$) HQS selection criterion (see Figure 3).

The X-ray logN-logS distribution shows slight evidence for the “bump” at $\sim 3 \times 10^{-11} \text{ erg s}^{-1} \text{ cm}^{-2}$ reported both by Maccacaro et al. (1989) and Nass et al. (1996),

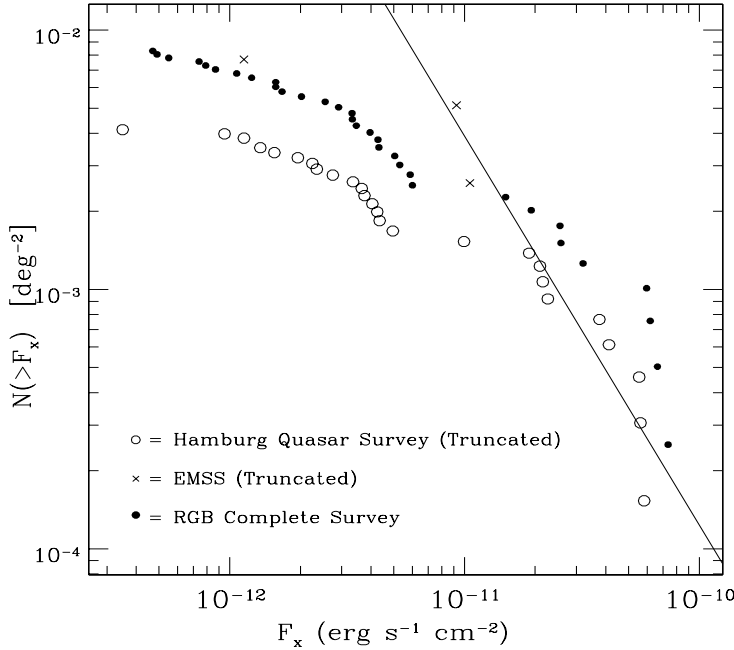


Fig. 7.— The X-ray logN-logS relationship for the RGB Complete, EMSS and HQS samples of BL Lacs. The latter two samples have been truncated to conform with the optical and radio selection criteria used in the creation of the RGB Complete sample. The solid line represents the no-evolution Euclidean $N \propto S^{-3/2}$ powerlaw arbitrarily normalized.

although the number statistics are poor. There also appears to be a rise in the surface density near $F_X = 8 \times 10^{-12} \text{ erg s}^{-1} \text{ cm}^{-2}$. The number statistics are better here, but it is still difficult to assess the significance of this feature. The distribution could alternately be characterized by a powerlaw with a deficit of sources near $5 - 10 \times 10^{-12} \text{ erg s}^{-1} \text{ cm}^{-2}$.

Bade et al. (1998b) have noted that the X-ray logN-logS distribution of HQS BL Lacs is more monotonic when extreme HBLs ($\alpha_{\text{ox}} < 0.91$) are excluded. From this, Bade et al. (1998b) infer that intermediate BL Lacs constitute the “basic BL Lac population” and that X-ray dominated BL Lacs are those objects which are observed in a state of enhanced X-ray activity. In order to test this hypothesis, we examined the RGB X-ray logN-logS distribution, excluding first those RGB BL Lacs with $\alpha_{\text{ox}} < 0.91$ as was done in Bade et al. (1998b). This criterion eliminates only two objects from the Complete sample, so the overall shape is not affected and the feature at $F_X = 8 \times 10^{-12} \text{ erg s}^{-1} \text{ cm}^{-2}$ remains. Even if we raise the cutoff to values of α_{ox} to 1.0, 1.1 or 1.2, the feature at $F_X \approx 8 \times 10^{-12} \text{ erg s}^{-1} \text{ cm}^{-2}$ remains although the number statistics necessarily deteriorate. This contradicts the result of Bade et al. (1998b), although we cannot rule it out because of the unknown effects of the optical magnitude limit on the RGB Complete sample. Therefore we find the feature at $F_X \approx 8 \times 10^{-12} \text{ erg s}^{-1} \text{ cm}^{-2}$ is significant, and does not seem to depend on properties of only an extreme subset of BL Lacs. We believe it therefore does not

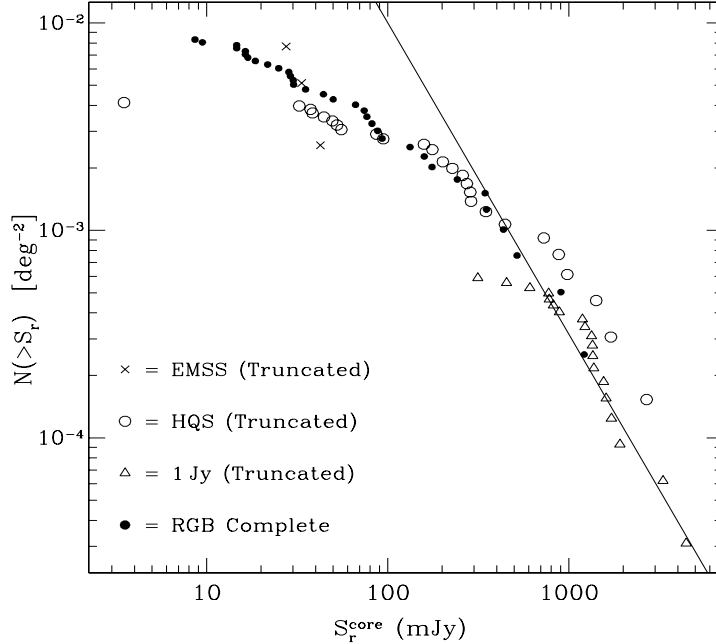


Fig. 8.— The radio logN-logS relationship for the RGB Complete, EMSS, HQS and 1 Jy samples of BL Lacs. The latter three samples have been truncated to conform with the selection criteria used in the creation of the RGB Complete sample. The solid line represents the no-evolution Euclidean $N(>S) \propto S^{-3/2}$ powerlaw arbitrarily normalized.

indicate extreme HBLs are objects in a state of enhanced X-ray activity, but suggest it is an indication of the type of breaks which are expected in logN-logS distributions of beamed objects (see below).

5.6. Radio logN–logS Relationship

Figure 8 shows a radio logN-logS distribution with the RGB, EMSS, HQS and 1 Jy samples included. As before, all samples have been truncated to include only those objects which adhere to the RGB selection criteria. This has the effect of reducing the 34 object 1 Jy complete sample to 19 objects. Note also that for all samples we plot core rather than total radio flux densities because the total emission contains kiloparsec-scale emission which is not as intimately connected with the relativistic flow in the center of the AGN. Many studies do not make this core vs. total flux distinction, but considering the wide range of core-to-lobe ratios exhibited by BL Lacs, we feel it important to do so here.

Several points are evident from the figure. The incompleteness of the 1 Jy sample below radio core flux densities of ~ 1 Jy is apparent from the turnover in the number counts in the diagram.

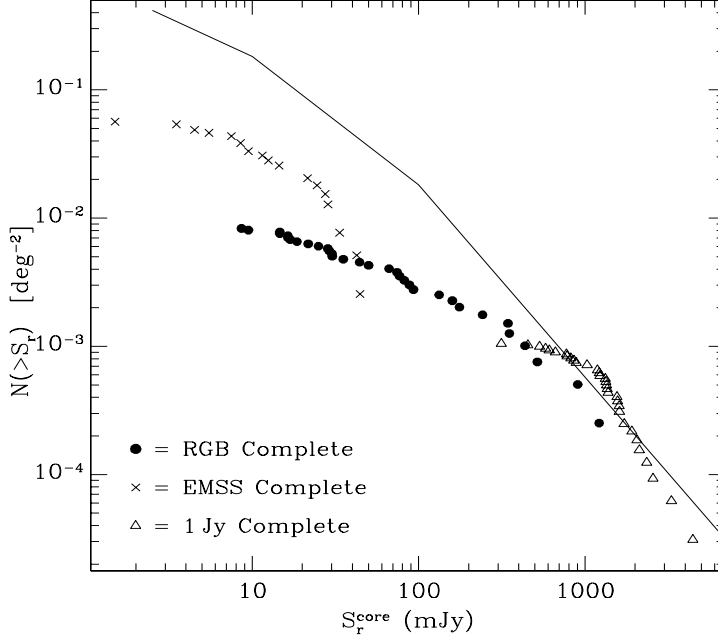


Fig. 9.— The radio logN-logS relationship for the RGB Complete, EMSS and 1 Jy samples of BL Lacs. The solid line represents the theoretical beaming model prediction of Urry, Padovani & Stickel (1991; §5.6).

However, above ~ 700 mJy the HQS, RGB and (to within $\sim 20\%$) the 1 Jy samples agree well, indicating that the effects of the X-ray flux and optical magnitude limits do not severely affect the RGB Complete sample at these high radio flux density limits. In the middle part of the diagram (~ 70 – 700 mJy), the RGB and HQS samples are roughly consistent with each other, unlike the results obtained for the X-ray logN-logS distribution. At the faintest radio flux densities, the surface density of HQS BL Lacs falls ~ 2 times below the RGB sample, indicating selection criteria based on identifying optically bright sources with flat values of α_{ox} produce an incompleteness that increases with decreasing radio flux density.

While it may be tempting to infer the evolutionary behavior of BL Lacs from the curvature of the RGB logN-logS distributions, it is dangerous to do so without careful modeling of the effects introduced by the X-ray and optical magnitude flux limits. This is illustrated in Figure 9 which shows the radio logN-logS distribution for the RGB Complete sample in comparison with the full (not truncated) 1 Jy and complete EMSS samples. Here the effects of the radio, optical and X-ray limiting flux densities inherent in the RGB catalog are clearly evident, particularly at low radio flux densities where the counts flatten appreciably, falling a factor of ~ 4 below the EMSS sample, which itself represents only a fraction of the radio faint BL Lac population.

Figure 9 also shows a theoretical beaming model for the logN-logS distribution (see and

Urry and Shafer 1984 and Urry et al. 1991 for details). This model is based on a simulation of a randomly oriented parent population of FR I radio galaxies which follow an assumed cosmological evolution model and whose jets have a powerlaw distribution of bulk jet Lorentz factors. The resulting BL Lac luminosity function is characterized by a double powerlaw, flattened by beaming at low radio powers with a break that is shifted to higher radio powers relative to breaks in the luminosity function of the parent population. When converted to surface number densities and fluxes, the $\log N$ - $\log S$ distribution of BL Lacs exhibits a Euclidean slope ($-3/2$) down to 100 mJy, flattens to $N(>S_r) \propto S_r^{-1}$ between $10 < S_r < 100$ mJy, and then becomes very flat ($\propto S_r^{-0.6}$) for $S_r < 10$ mJy. Beaming therefore tends to flatten source counts to an increasing degree at lower flux densities.

Unfortunately, because neither the EMSS nor RGB samples are truly complete (containing *all* BL Lacs) at radio flux densities below ~ 1 Jy, it is not possible to directly compare the specific predictions of this model with any of the samples in Figure 9 other than the 1 Jy which provides the normalization. However, we can make some general observations. The RGB sample follows a Euclidean slope above ~ 200 mJy. At intermediate radio flux densities, it flattens more than the model but, as stated above, this is at least partly a result of the incompleteness caused by the RGB Complete sample’s flux limits. At ~ 40 mJy, the surface density of the RGB and EMSS samples coincide, but below ~ 20 mJy, the Complete EMSS (HBL) sample quickly overwhelms the RGB sample. Nevertheless, the EMSS sample falls well below the prediction of Urry et al. (1991). It is this deficit of low flux/luminosity BL Lacs which led Morris et al. (1991) to postulate that HBLs may evolve negatively, a claim reinforced by Rector et al. (1999a) in their new analysis of the V/V_{\max} analysis of an updated Complete EMSS sample. However, the EMSS survey consists of only the most extreme X-ray-dominated objects. As discussed below, we believe the dichotomy of HBLs and LBLs is a result of selection effects and conclusions drawn about the evolution of only one extreme end of the distribution should therefore be treated cautiously.

6. Discussion

6.1. Comparison with Previous BL Lac Surveys

The principal result of this study is that the RGB BL Lacs exhibit a continuous range in SEDs rather than segregating into two distinct classes: HBLs vs. LBLs (or XBLs vs. RBLs). Clearly the RGB sample smoothly spans a vast range of SEDs: 5 orders of magnitude in S_x/S_r , $0.5 < \alpha_{ox} < 1.7$ and $0.2 < \alpha_{ro} < 0.8$. Most RGB BL Lacs have intermediate properties (e.g., S_x/S_r ratios) between the HBL and LBL extremes that dominated earlier samples. Similar preliminary results have also been reported for the deep DXRBS and REX X-ray surveys (Perlman et al. 1998; Caccianiga et al. 1999). The question remains whether these results are an accurate representation of the BL Lac population as a whole, or whether the true BL Lac distribution is bimodal and the flux limits of the RGB survey unfortunately tuned to make it particularly sensitive to objects with

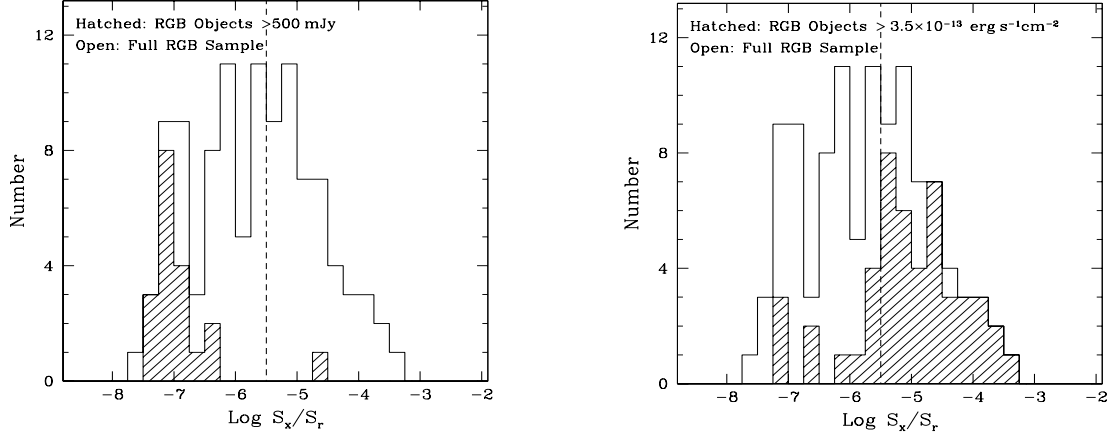


Fig. 10.— Comparison of the $\log S_x/S_r$ ratio for the full RGB sample (upper solid line) and those objects with **a.** radio flux densities greater than 500 mJy (hatched histogram) or **b.** X-ray fluxes greater than $3.5 \times 10^{-13} \text{ erg s}^{-1} \text{cm}^{-2}$. Note the similarity between the hatched distributions and those in Figure 4.

intermediate SEDs. Occam’s Razor makes it tempting to hypothesize that the intermediate nature of the RGB sample is an accurate reflection of an underlying unimodal distribution and that the previously observed bimodal distribution is a result of high flux limits of previous surveys, but this hypothesis bears closer examination.

Figure 10 shows what the RGB’s distribution of S_x/S_r ratios would have been had either the radio (Fig. 10a) or X-ray (Fig. 10b) flux limits been higher. Not surprisingly, increasing the radio flux limit preferentially selects increasingly more radio-dominant BL Lacs. At a limiting radio flux density of 500 mJy a distribution roughly consistent with that of the 1 Jy sample (Fig. 4) results. (Too few RGB objects are brighter than 1 Jy to make a meaningful comparison at this higher radio flux density limit.) Direct comparisons with X-ray-selected samples are complicated since none of the comparison surveys were conducted over the same energy band as the RGB (0.1–2.4 keV with the ROSAT PSPC) and X-ray flux limits are sensitive to the assumed photon index and Galactic column density. In addition, the Slew Survey has a factor of several range of limiting sensitivities while the HEAO-1 sample is a result of a flux density (not flux) limited survey complicating a precise comparison with the RGB sample.

Despite these ambiguities, increasing the limiting X-ray flux of the RGB survey selects the more X-ray-dominated RGB BL Lacs and at a flux limit of $3.5 \times 10^{-12} \text{ erg s}^{-1} \text{cm}^{-2}$, the distribution is roughly consistent with both the HEAO-1 and Slew Survey distributions (Figs. 4a and 4b). However, the effective limit of the EMSS in the ROSAT band is $2.2 - 3.5 \times 10^{-2} \mu\text{Jy}$ (T. Rector, private communication) which is only marginally brighter than the RGB X-ray flux limit. Therefore if our assumption of a unimodal S_x/S_r ratio for BL Lacs is correct, then we predict (based on only a small difference in the RGB and EMSS X-ray survey flux limits), that the EMSS

sample should closely resemble that of the RGB; this clearly is not the case. However, Rector et al. (1999a) have made a careful re-examination of the EMSS identifications and have found several new BL Lacs that were misidentified because of their strong 4000 Å break contrasts. The addition of these sources does bring the EMSS and RGB S_x/S_r distributions into somewhat closer agreement. Also, a new analysis by Rector et al. (1999b) which extends the complete EMSS sample down to $2.0 \times 10^{-13} \text{ erg s}^{-1} \text{cm}^{-2}$ and declinations $>40^\circ$, also preferentially adds objects with intermediate S_x/S_r ratios, but not sufficiently to make the RGB and EMSS distributions consistent. Nevertheless, agreement between the 1 Jy, HEAO-1 and Slew samples with that of the RGB sample were either its radio or, respectively, X-ray flux limits raised, is compelling.

Another demonstration that the RGB survey likely accurately reflects an underlying unimodal distribution arises from the following Monte Carlo simulation. We create hypothetical populations of BL Lacs where both radio and X-ray $\log N - \log S$ distributions obey simple powerlaws, and radio and X-ray fluxes are independent variables. The first assumption is clearly an oversimplification since there is ample evidence for breaks in both the radio and X-ray $\log N - \log S$ relationships (including this paper) but including these breaks would introduce many new parameters to the model (location of the break(s) and the slopes above and below them) without adding substantially to the general sense of the results. Figure 11 shows a simulation of 30,000 sources whose radio and X-ray fluxes are constrained to be $>1 \text{ mJy}$ and $>5 \times 10^{-14} \text{ erg s}^{-1} \text{cm}^{-2}$, respectively. These limits were chosen because they are fainter than either the radio or X-ray flux of any BL Lac in any of the relevant comparison samples (EMSS, RGB or 1 Jy). We then applied the different flux limits of the comparison surveys and randomly chose objects in order to create samples with the same number of objects. The particular simulation shown assumed the $\log N - \log S$ powerlaw slopes were -1.2 and -0.8 in the radio and X-ray, respectively. (See Urry, Padovani & Stickel 1991 and Maccacaro et al. 1984 for the relevance of these specific indices.)

Clearly Figure 11 suggests the underlying distribution is unimodal; this is, in fact, a universal among all the simulations, although the location of the peak in the distributions varies with the radio and X-ray $\log N - \log S$ slopes. The distribution shown in Figure 11 peaks at $\log S_x/S_r = -5.61$. The distributions resulting from flux limits at 1 Jy ($5 \times 10^{-13} \text{ erg s}^{-1} \text{cm}^{-2}$) are acceptably consistent with the distributions shown in Figure 4 for the 1 Jy (EMSS) samples while the sample created by enforcing a radio flux limit of 20 mJy and an X-ray flux limit of $3 \times 10^{-13} \text{ erg s}^{-1} \text{cm}^{-2}$ is an acceptable match to the RGB sample's distribution, given the simplicity of our assumptions.

Both the above analyses strongly point towards the simple conclusion that the true distribution of BL Lac SEDs, and S_x/S_r ratios in particular, is unimodal and accurately represented by the RGB survey. Our results also show that the previously observed bimodality can be explained as a result of naturally occurring observational selection effects present in older surveys. A similar conclusion is reached by Caccianiga et al. (1999) in their preliminary examination of the REX survey BL Lacs and in the theoretical modeling of Fossati et al. (1997).

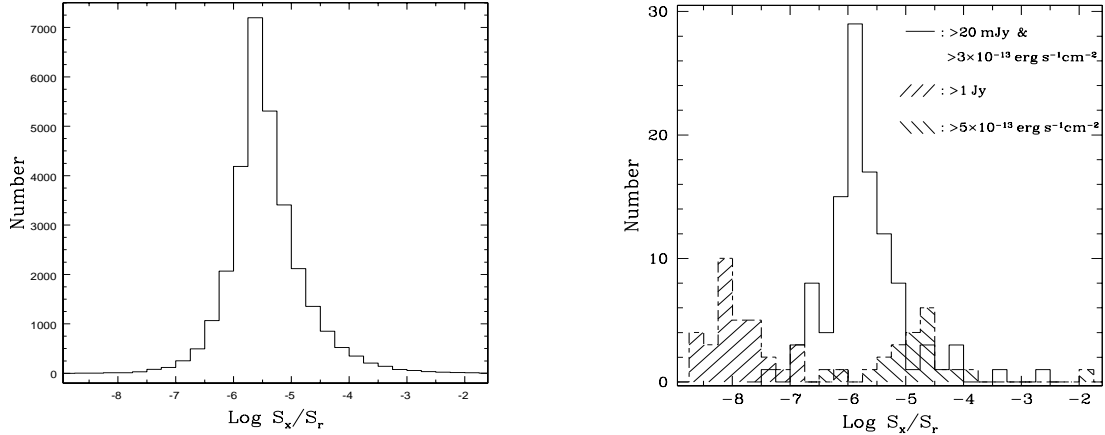


Fig. 11.— Results of a Monte Carlo simulation of the $\log S_x/S_r$ for BL Lacs. The model shown assumes the $\log N - \log S$ relationship follows a $S^{-1.2}$ powerlaw in the radio and a $S^{-0.8}$ powerlaw in the X-ray. **a.** The underlying distribution which is unimodal and peaks at $\log S_x/S_r = -5.6$ **b.** The distributions which would result from this sample if surveys with flux limits of 1 Jy (right-slanted hatched histogram), $5 \times 10^{-13} \text{ erg s}^{-1} \text{ cm}^{-2}$ (left-slanted hatched histogram) or dual flux limits of 20 mJy and $3 \times 10^{-13} \text{ erg s}^{-1} \text{ cm}^{-2}$ were performed. Flux limits have been chosen based on the limits inherent in the 1 Jy, EMSS and RGB surveys, respectively and the total number of objects in these simulated samples have been matched to the number of objects in the survey they are intended to represent. Although the agreement is not perfect, the similarity with Figure 4 is suggestive that the $\log S_x/S_r$ distribution for BL Lacs is unimodal and the bimodal distribution reflected in the EMSS and 1 Jy samples is a result of the flux limits of these different surveys.

6.2. A Unified BL Lac Population

Differences between the various subclasses of BL Lacs have been attributed to different jet orientations to the line-of-sight (e.g., Kollgaard 1994; Urry and Padovani 1995). However, further analysis showed that the range of SEDs observed in LBLs and HBLs cannot be reproduced by simple changes in jet orientation (e.g., Sambruna et al. 1996; Fossati et al. 1997) and our results confirm this (§5). Padovani and Giommi (1995a) propose an alternative to this orientation-based model, namely, that LBLs and HBLs essentially share the same range in orientation, but have intrinsically different SEDs. They postulate that the frequency at which the synchrotron break occurs, ν_{break} , differs intrinsically in LBLs and HBLs. This then alters the balance of synchrotron and inverse Compton emission present in soft X-rays, moving the objects in the $\alpha_{\text{ro}} - \alpha_{\text{ox}}$ diagram. This model predicts that BL Lacs whose spectra break at high frequencies should be HBL-like and lie along the horizontal path labeled “HBLs” in Figure 3. Objects with ν_{break} at low frequencies should lie along the diagonal swath labeled “LBLs” in the $\alpha_{\text{ro}} - \alpha_{\text{ox}}$ plane. Assuming $\langle \alpha_{\text{ox}} \rangle \simeq 0.7$ and $\langle \alpha_{\text{ro}} \rangle \simeq 0.37$, as derived from the EMSS sample, and a spectral index $\alpha_{\text{break}} \simeq 1.9$, valid for $\nu > \nu_{\text{break}}$, Padovani and Giommi (1995a) were able to reproduce the bimodal locations of the EMSS XBLs

and 1 Jy RBLs in the color-color diagram. If this model is correct, then all new BL Lacs should continue to reside along constrained loci in the $\alpha_{\text{ro}}-\alpha_{\text{ox}}$ plane, although this SED-based model need not lead to a bimodal separations of classes. Our results show that this may be the case with the RGB objects following the traditional paths in the α_{ro} vs. α_{ox} plane, although the scatter is significant and the triple-flux limits restrict the range of SEDs to which we are sensitive.

Two additional new unification models attempt to explain the physical origin of the wide range of SEDs in BL Lacs. The first asserts that the shape of the SED is linked to the bolometric luminosity (Fossati et al. 1997). In this model, HBLs and LBLs are manifestations of the same phenomenon, but the broadband SED varies in a predictable way with bolometric luminosity. This model can reproduce the disparate distribution of the 1 Jy and Slew Survey samples in the $\alpha_{\text{ro}}-\alpha_{\text{ox}}$ plane, and predicts an intrinsically smooth transition between the two extremes. The other model predicts that the origin of the SED differences lies in differences in the electron kinetic luminosity of the jet which is related to jet size ($L_{\text{jet}} \propto r^2$; Georganopoulos and Marscher 1998). This model also predicts a smooth transition between the previously disparate BL Lac subclasses which qualitatively agrees with the distribution of RGB objects. Quantitative comparison of these models with our data is, however, difficult both because the RGB sample is triply flux limited and because the RGB Complete sample's limiting magnitude of 18.0 curtails the range of possible SEDs to which the sample is sensitive. We are however currently attempting to model the selection effects, but extending the Complete sample to a fainter magnitude limit would clearly alleviate some restrictions.

The wide range of spectral indices exhibited by the RGB BL Lacs has important implications for followup surveys for RASS BL Lacs. Figure 3 shows not only the distribution of BL Lacs in the $\alpha_{\text{ro}}-\alpha_{\text{ox}}$ diagram, but also the color-color classification boundaries established in the EMSS by Stocke et al. (1991). These regions have been used to successfully identify new BL Lac objects. Nearly all Einstein Slew Survey objects in the region defined by $\alpha_{\text{ro}}=(0.3,0.6)$ and $\alpha_{\text{ox}}=(0.55,1.2)$ were spectroscopically confirmed as BL Lacs (Schachter et al. 1993b; Perlman et al. 1996a). A criterion of $\alpha_{\text{ox}} < 1.1$ was used to select candidates for the Hamburg Quasar Survey BL Lac sample (Nass et al. 1996). However, the RGB sample, selected without any spectral index criteria, shows that targeting only those objects in the RASS with particular color-color indices will miss a large fraction of the BL Lacs. If, for example, the EMSS BL Lac class boundaries had been used to select candidates, 67% of the RGB BL Lacs would have been excluded (70% of the sources in our Complete sample). Using the criterion in Nass et al. (1996) would have excluded 70% of our objects (and 76% of objects in the Complete sample). Therefore while the likelihood of finding BL Lacs does increase dramatically with decreasing α_{ox} , candidates cannot be chosen based on their SEDs without producing highly biased samples leading to incorrect or uncertain conclusions.

Finally, because we lack detailed knowledge of the effects of the triple flux limits on the characteristics of the entire RGB BL Lac sample, we are not at present able to definitively evaluate the predictions of any of the FR I/BL Lac or HBL/LBL unification models. Some insights might be obtained with Monte Carlo simulations which exclude sources which fall below our RGB flux

limits, but this, of course, requires a more elaborate simulation of the intrinsic properties of the BL Lac population than the simple simulation shown in Figure 11. Two additional approaches can be pursued. First, redshifts for the RGB Complete Sample can be obtained with currently available optical telescopes. This would transform the source counts into correctly normalized luminosity functions, which could then be compared with luminosity functions of FRI radio galaxies. But here again, the selection effects must be precisely taken into account. Second, the RGB sample can be extended to reduce the effects of the flux limits. Most importantly, spectra should be obtained for RGB objects fainter than ~ 18.5 in order to discriminate BL Lacs from other X-ray/radio sources. While improvements in the X-ray flux limit the RGB catalog are not likely in the near future, the NVSS (Condon et al. 1998) and FIRST (Becker et al. 1995) radio surveys permit a factor of $\simeq 20$ reduction in the radio flux limit. BL Lac samples based on these radio surveys are currently being pursued (Caccianiga et al. 1999; Laurent-Muehleisen et al. 1999). Here again, substantial spectroscopy of optically faint objects will be needed. Significant progress in refining BL Lac unification scenarios thus depends on spectroscopy with new 8-meter class telescopes, which fortunately are proliferating today.

We wish to thank Nahum Arav, Michael Brotherton and the referee, Simon Morris, for a variety of useful comments which greatly improved the final manuscript. This work was partially supported by NASA under Grant NAGW-2120 to EDF and partially by the Department of Energy at the Lawrence Livermore National Laboratory under contract W-7405-ENG-48. RIK acknowledges support by Fermi National Accelerator Laboratory under the U. S. Department of Energy contract No. DE-AC02-76CH03000. We have made use of the NASA/IPAC Extragalactic Database, operated by the Jet Propulsion Laboratory, California Institute of Technology, under contract with NASA. SALM also acknowledges partial support from the NASA Space Grant Consortium through their Space Grant Fellow program and the NSF (grant AST-98-02791).

References

Angel, J. R. P., and Stockman, H. S. 1980, *ARA&A*, 18, 321

Antonucci, R. R. J. 1993, *ARA&A*, 31, 473

Bade, N., Fink, H. H., and Engels, D. 1994, *A&A*, 286, 388

Bade, N., Engels, D., Voges, W., Beckmann, V., Boller, T., Cordis, L., Dahlem, M., Englhauser, J., Molthagen, K., Nass, P., Studt, J., and Reimers, D. 1998a, *A&A*, 127, 145

Bade, N., Beckmann, V., Douglas, N. G., Barthel, P. D., Engels, D., Cordis, L., Nass, P., and Voges, W. 1998b, *A&A*, 334, 459

Becker, R. H., White, R. L., and Helfand, D. J. 1995, *ApJ*, 450, 559

Beckmann, V. 1999, in BL Lac Phenomenon, proceedings from the meeting held in Turku, Finland, June 22-26, 1998, p. (in Press, astro-ph/9810154)

Blandford, R. D., and Rees, M. J. 1978, in Pittsburgh Conference on BL Lac Objects, ed. A. M. Wolfe (University of Pittsburgh, Pittsburgh), p. 328

Bregman, J. N., Maraschi, L., and Urry, C. M. 1987, in Scientific Accomplishments of *IUE*, ed. Y. Kondo (Dordrecht: Reidel), p. 685

Brinkmann, W., Siebert, J., Reich, W., Fürst, E., Reich, P., Voges, W., Trümper, J., and Wielebinski, R. 1995, *A&AS*, 109, 147

Brinkmann, W., Siebert, J., Kollgaard, R. I., and Thomas, H.-C. 1996, *A&A*, 313, 356

Brinkmann, W., Siebert, J., Feigelson, E. D., Kollgaard, R. I., Laurent-Muehleisen, S. A., Reich, P., Voges, W., Trümper, J., and McMahon, R. 1997, *A&A*, 323, 739

Browne, I. W. A. 1983, *MNRAS*, 204, 23P

Browne, I. W. A., and Marchā, M. J. M. 1993, *MNRAS*, 261, 795

Caccianiga, A., Maccacaro, R., Wolter, A., Della Ceca, R., and Gioia, I. M. 1999, *ApJ*, 513, 51

Condon, J. J., Cotton, W. D., Greisen, E. W., Yin, Q. F., Perley, R. A., Taylor, G. B., and Broderick, J. J. 1998, *AJ*, 115, 1693

Elvis, M., Plummer, D., Schachter, J., and Fabbiano, G. 1992, *ApJS*, 80, 257

Fanaroff, B., and Riley, J. M. 1974, *MNRAS*, 167, 31P

Feigelson, E. D., and Nelson, P. I. 1985, *ApJ*, 293, 192

Fischer, J.-U., Hasinger, G., Schwope, A. D., Brunner, H., Boller, T., Trümper, J., Voges, W., and Neizvestny, S. 1998, *Astron. Nachr.* (Submitted), astro-ph/9811139

Fleming, T. A., Green, R. F., Jannuzi, B. T., Liebert, J. Smith, P. S., and Fink, H. 1993, *AJ*, 106, 1729

Fossati, G., Cellotti, A., Ghisellini, G., and Maraschi, L. 1997, *MNRAS*, 289, 136

Georganopoulos, M., and Marscher, A. P. 1998, *ApJ*, 506, 621

Ghisellini, G., Maraschi, L., and Treves, A. 1985, *A&A*, 146, 204

Ghisellini, G., Padovani, P., Celotti, A., and Maraschi, L. 1993, *ApJ*, 407, 65

Gioia, I., Maccacaro, T., Schild, R., Wolter, A., Stocke, J., Morris, S., and Henry, J. P. 1990, *ApJS*, 72, 567

Giommi, P., and Padovani, P. 1994, *MNRAS*, 268, L51

Gregory, P. C., Scott, W. K., Douglas, K., and Condon, J. J. 1996, *ApJS*, 103, 427

Hagen, H. J., Groote, D., Engels, D., and Reimers, D. 1995, *A&AS*, 111, 195

Henstock, D. R., Browne, I. W. A., Wilkinson, P. N., and McMahon, R. G. 1997, *MNRAS*, 290, 380

Jannuzi, B. T., Smith, P. S., and Elston, R. 1994, *ApJ*, 428, 130

Kibblewhite, E. J., Bridgeland, M. T., Bunclark, P. A., and Irwin, M. J. 1984, *Astronomical Microdensity Conference*, NASA-2317, 277

Kock, A., Meisenheimer, K., Brinkmann, W., Neumann, M., and Siebert, J. 1996, *A&A*, 307, 745

Kollgaard, R. I. 1994, *Vistas in Astronomy*, 38, 29

Kollgaard, R. I., Wardle, J. F. C., Roberts, D. H., and Gabuzda, D. C. 1992, *AJ*, 104, 1687

Kollgaard, R. I., Gabuzda, D. C., and Feigelson, E. D. 1996a, *ApJ*, 460, 174

Kollgaard, R. I., Palma, C., Laurent-Muehleisen, S. A., and Feigelson, E. D. 1996b, *ApJ*, 465, 115

Kollgaard, R. I., Gabuzda, D. C., Laurent-Muehleisen, S. A., and Feigelson, E. D. 1999, (in preparation)

Lamer, G., Brunner, H., and Staubert, R. 1996, *A&A*, 311, 384

Laurent-Muehleisen, S. A. 1996, PhD Thesis, The Pennsylvania State University

Laurent-Muehleisen, S. A., Kollgaard, R. I., Moellenbrock, G. A., and Feigelson, E. D. 1993, *AJ*, 106, 875

Laurent-Muehleisen, S. A., Kollgaard, R. I., Ryan, P. J., Feigelson, E. D., Brinkmann, W., and Siebert, J. 1997, *A&AS*, 122, 235

Laurent-Muehleisen, S. A., Kollgaard, R. I., Ciardullo, R. B., Feigelson, E. D., Brinkmann, W., and Siebert, J. 1998, *ApJS*, 118, 127

Laurent-Muehleisen, S. A., Becker, R. H., White, R. L., and Helfand, D. J. 1999, *ApJ*, (in preparation)

LaValley, M., Isobe, T., and Feigelson, E. D. 1992, *BAAS*, 24, 839

Maccacaro, R., Gioia, I. M., Schild, R. E., Wolter, A., Morris, S. L., and Stocke, J. T. 1989, in *BL Lac Objects*, ed. L. Maraschi, T. Maccacaro and M.-H. Ulrich (Berlin: Springer Verlag), p. 222

Maccacaro, T., Gioia, I. M., Maccagni, D., and Stocke, J. T. 1984, *ApJ*, 284, L23

Maccacaro, T., Wolter, A., McLean, B., Gioia, I. M., Stocke, J. T., Della Ceca, R., Burg, R., and R., F. 1994, *ApJLett Commun.*, 29, 267

Marchā, M. J. M., Browne, I. W. A., Impey, C. D., and Smith, P. S. 1996, *MNRAS*, 281, 425

Morris, S. L., Stocke, J. T., Gioia, I. M., Schild, R. E., Wolter, A., Maccacaro, T., and Della Ceca, R. 1991, *ApJ*, 380, 49

Nass, P., Bade, N., Kollgaard, R. I., Laurent-Muehleisen, S. A., Reimers, D., and Voges, W. 1996, *A&A*, 309, 419

Neumann, M., Reich, W., Fürst, E., Brinkmann, W., Reich, P., Siebert, J., Wielebinski, R., and Trümper, J. 1994, *A&AS*, 106, 303

Padovani, P., and Giommi, P. 1995a, *ApJ*, 444, 567

Padovani, P., and Giommi, P. 1995b, *MNRAS*, 277, 1477

Perlman, E. S., and Stocke, J. T. 1993, *ApJ*, 406, 430

Perlman, E. S., Stocke, J. T., Schachter, J. F., Elvis, M., Ellingson, E., Urry, C. M., Potter, M., Impey, C. D., and Kolchinsky, P. 1996a, *ApJS*, 104, 251

Perlman, E. S., Stocke, J. T., Wang, Q. D., and Morris, S. L. 1996b, *ApJ*, 456, 451

Perlman, E. S., Padovani, P., Giommi, P., Sambruna, R. M., Jones, L. R., Tzioumis, A., and Reynolds, J. 1998, *AJ*, 115, 1253

Rector, T. A., Stocke, J. T., and Perlman, E. S. 1999a, *ApJ*, (In Press)

Rector, T. A., Stocke, J. T., Perlman, E. S., Morris, S. L., and Gioia, I. M. 1999b, *ApJ*, (in preparation)

Remillard, R. A., Bradt, H. V., Buckley, D. A. H., Roberts, W., Schwartz, D. A., Tuohy, I. R., and Wood, K. 1986, *ApJ*, 301, 742

Sambruna, R. M., Maraschi, L., and Urry, C. M. 1996, *ApJ*, 463, 444

Scarpa, R., and Falomo, R. 1997, *A&A*, 325, 109

Schachter, J. F., Elvis, M., and Szentgyorgyi, A. 1993a, *BAAS*, 25, 1447

Schachter, J. F., Stocke, J. T., Perlman, E., Elvis, M., Remillard, R., Granados, A., Luu, J., Huchra, J. P., Humphreys, R., Urry, C. M., and Wallin, J. 1993b, *ApJ*, 412, 541

Schwartz, D. A., Brissenden, R. J. V., Tuohy, I. R., Feigelson, E. D., Hertz, P. L., and Remillard, R. A. 1989, in *BL Lac Objects*, ed. L. Maraschi, T. Maccacaro and M.-H. Ulrich (Berlin: Springer Verlag), p. 209

Stein, W. A., O'Dell, S. L., and Strittmatter, P. A. 1976, *ARAA*, 14, 173

Stickel, M., Padovani, P., Urry, C. M., Fried, J. W., and Kühr, H. 1991, *ApJ*, 374, 431

Stocke, J. T., and Rector, T. A. 1997, *ApJLett*, 489, L17

Stocke, J. T., Morris, S. L., Gioia, I. M., Maccacaro, T., Schild, R. E., and Wolter, A. 1989, in *BL Lac Objects*, ed. L. Maraschi, T. Maccacaro and M.-H. Ulrich (Berlin: Springer Verlag), p. 242

Stocke, J. T., Morris, S. L., Gioia, I., Maccacaro, T., Schild, R. E., and Wolter, A. 1990, *ApJ*, 348, 141

Stocke, J. T., Morris, S. L., Gioia, I. M., Maccacaro, T., Schild, R., Wolter, A., Fleming, T. A., and Henry, J. P. 1991, *ApJS*, 76, 813

Urry, C. M., and Padovani, P. 1995, *PASP*, 107, 803

Urry, C. M., and Shafer, R. A. 1984, *ApJ*, 280

Urry, C. M., Padovani, P., and Stickel, M. 1991, *ApJ*, 382, 501

Urry, C. M., Sambruna, R. M., Worrall, D. M., Kollgaard, R. I., Feigelson, E. D., Perlman, E. S., and Stocke, J. T. 1996, *ApJ*, 463, 424

Vermeulen, R. C., Taylor, G. B., Readhead, A. C. S., and Browne, I. W. A. 1996, *AJ*, 111, 1013

Wardle, J. F. C., Moore, R. L., and Angel, J. R. P. 1984, *ApJ*, 279, 93

Wood, K. S., Meekins, J. F., Yentis, D. J., Smathers, H. W., McNutt, D. P., Bleach, R. D., Friedman, H., Byram, E. T., Chubb, T. A., and Meidav., M. 1984, *ApJS*, 56, 507

Wurtz, R., Stocke, J. T., and Yee, H. K. C. 1996, *ApJS*, 103, 109

TABLE 2
RGB BL LAC SOURCE PROPERTIES

RGB J Name	Alternate Name	RA (J2000)	Dec	S_5^{core} (mJy)	F_X ($10^{-12} \frac{\text{erg}}{\text{s cm}^2}$)	O (mag)	α_x	α_{ro}	α_{ox}	z	Ref.
0007+472	RX J00079+4711	00 07 59.97	47 12 07.8	67	1.43	18.8 ^a	...	0.50	1.15	0.280	K96,L97
0035+598	1ES 0033+595	00 35 52.63	59 50 04.6	49	26.4	20.0 ^a	...	0.58	0.54	...	PG95,L97
0040+408 ^b	B3 0037+405	00 40 13.81	40 50 04.7	10	2.03	20.3 ^a	...	0.47	0.89	...	PG95,L97
0109+182 ^d	RX J01090+1815	01 09 08.2	18 16 08	82	8.74	17.1	0.94	0.40	1.06	...	B97,L97,F98
0110+418 ^b	RX J01100+4149	01 10 04.79	41 49 50.9	18	2.53	18.4 ^c	1.11	0.37	1.10	0.096	L98,B97,L97
0112+227	S2 0109+22	01 12 05.82	22 44 38.8	700	3.56	15.6	1.96	0.46	1.66	...	B95,B97,VLA
0115+253 ^{b,d}	RX J01157+2519	01 15 46.5	25 19 56	27	4.89	19.3	0.84	0.47	0.82	...	N96,B97,L97
0123+343 ^d	1ES 0120+340	01 23 08.8	34 20 50	40	53.4	16.8	1.24	0.30	0.89	0.272	PG95,B97,L97
0136+391 ^d	B3 0133+388	01 36 32.7	39 06 00	49	20.8	15.8	1.16	0.25	1.16	...	L98,B97,L97
0152+017 ^{b,d}	PMN J0152+0146	01 52 39.60	01 47 17.2	65	5.56	17.0 ^c	1.48	0.37	1.27	0.080	L98,B97,L97
0153+712 ^b	8C 0149+710	01 53 25.85	71 15 06.5	291	3.05	17.7 ^{a,c}	...	0.56	1.19	0.022	M96,L97
0202+088 ^{b,d}	PMN J0202+0848	02 02 26.5	08 49 14	62	2.87	20.0	1.36	0.60	0.91	...	N96,B97,L97
0214+517	RX J 02142+5144	02 14 17.93	51 44 52.0	161	12.7	17.9 ^{a,c}	1.04	0.52	0.91	0.049	M96,L97
0227+020 ^b	RX J02272+0201	02 27 16.58	02 02 00.1	9	24.2	20.2	0.90	0.45	0.46	...	N96,B97,L97
0250+172	RX J02506+1712	02 50 37.96	17 12 08.5	35	5.71	17.5	1.02	0.35	1.09	...	L98,B97,L97
0314+247 ^{b,d}	RX J03140+2445	03 14 02.7	24 44 31	6	1.44	18.3 ^c	...	0.28	1.22	0.054	L98,L97
0316+090 ^d	RX J03161+0904	03 16 12.8	09 04 43	51	3.96	18.8	3.28	0.49	1.64	...	B97,L97,F98
0321+236	RX J03219+2336	03 21 59.93	23 36 11.0	56	0.65	16.8	...	0.34	1.55	...	L98,L97
0326+024 ^d	1H 0323+022	03 26 13.97	02 25 14.7	68	17.8	17.5	1.27	0.41	0.97	0.147	B95,L98,L96,L97
0416+010	1H 0414+009	04 16 52.49	01 05 24.0	48	70.8	16.9	1.55	0.33	0.90	0.287	B95,L96,L97
0424+006	PKS J0424+0036	04 24 46.84	00 36 06.3	1100	1.41	17.3	...	0.63	1.36	...	B95,VLA
0450+450 ^b	1ES 0446+449	04 50 07.24	45 03 11.9	4	7.46	19.0 ^a	...	0.29	0.87	0.203?	PG95,L97
0505+042	PMN J0505+0416	05 05 34.78	04 15 54.7	90	7.61	17.6	1.35	0.44	1.10	...	L98,B97,L97
0507+676	1ES 0502+675	05 07 56.18	67 37 24.3	21	38.4	17.5 ^a	...	0.31	0.83	...	B95,L97

TABLE 2—Continued

RGB J Name	Alternate Name	RA (J2000)	Dec	S_{ν} (mJy)	F_X ($10^{-12} \frac{\text{erg}}{\text{s cm}^2}$)	O (mag)	α_x	α_{ro}	α_{ox}	z	Ref.
0650+250 ^d	1ES 0647+250	06 50 46.5	25 03 00	85	44.1	15.8 ^a	...	0.30	1.05	...	B95,L97
0654+427 ^b	B3 0651+428	06 54 43.53	42 47 58.7	134	0.96	18.1 ^c	2.59	0.52	1.72	0.126	M96,L97
0656+426 ^b	4C+42.22	06 56 10.66	42 37 02.4	138	3.87	16.5 ^c	2.18	0.40	1.60	0.059	L98,B97,L97
0753+538	4C+54.15	07 53 01.38	53 52 59.6	907	0.97	18.2	...	0.68	1.29	>0.200	B95,L97
0757+099	PKS J0757+0956	07 57 06.64	09 56 34.9	1250	2.18	15.9	...	0.50	1.48	0.660?	B95,VLA
0809+523	1ES 0806+524	08 09 49.19	52 18 58.4	123	19.1	15.5 ^a	2.18	0.31	1.49	0.138	B95,B94,L97,B98
0814+296 ^d	EXO 0811.2+2949	08 14 21.29	29 40 21.1	20	1.91	17.9	...	0.34	1.23	...	PG95,L97
0831+044	OJ 49	08 31 48.88	04 29 39.1	1000	1.27	16.0	...	0.52	1.56	0.180	B95,VLA
0854+441	B3 0850+443	08 54 09.88	44 08 30.3	31	3.31	17.6	1.80	0.35	1.34	...	N96,L98,B97,L97
0854+201	OJ 287	08 54 48.87	20 06 30.6	2300	3.59	15.6 ^a	1.60	0.55	1.55	0.306	B95,U96,G93
0915+295	B2 0912+29	09 15 52.40	29 33 24.0	172	10.1	16.3	1.31	0.40	1.23	...	B95,L96,L97
0916+526 ^b	RX J09168+5238	09 16 51.92	52 38 28.4	46	5.35	17.4	1.18	0.37	1.14	0.190	N96,L97,B98
0928+747	8C 0923+750	09 28 02.97	74 47 19.1	5	1.98	21.0	0.78	0.43	0.72	0.638	B95,P96,L97
0929+502 ^b	RX J09292+5013	09 29 15.44	50 13 36.0	895	1.19	17.2	1.30	0.60	1.43	...	N96,B97,L97
0930+350 ^b	7C 0927+3516	09 30 55.28	35 03 37.6	337	0.71	20.4	...	0.77	1.03	...	H97,L97
0952+656	RX J09524+6538	09 52 32.19	65 38 01.1	27	1.41	18.0	1.23	0.37	1.27	...	L98,B97,L97
1000+225A	4C+22.25	10 00 21.36	22 33 07.4	≤5	0.96	17.8	...	<0.20	1.35	0.419	B95,L97
1012+424 ^b	B3 1009+427	10 12 44.30	42 29 57.2	29	7.68	18.1	0.84	0.39	0.92	...	L98,B97,L97
1015+494	1H 1011+496	10 15 04.17	49 26 00.6	242	19.5	16.5	1.49	0.44	1.14	0.2?	B95,L96,L97
1047+546 ^b	1ES 1044+549	10 47 45.82	54 37 41.3	6	0.45	21.2	0.63	0.49	0.89	...	PG95,B97,L97
1053+494 ^b	MS 1050.7+4946	10 53 44.14	49 29 56.1	19	1.20	17.5 ^c	1.62	0.30	1.46	0.140	R99,B97,L97
1104+382	MKN 421	11 04 27.31	38 12 31.8	600	405.	13.3	1.37	0.28	1.11	0.031	B95,L96,VLA
1120+422	1ES 1118+424	11 20 48.07	42 12 12.5	19	6.65	17.1	1.30	0.27	1.18	0.124?	PG95,L98,B97,L97
1149+246 ^d	EXO 1149.9+2455	11 49 30.3	24 39 27	15	9.12	18.9	...	0.39	0.85	...	PG95,L97
1209+413	B3 1206+416	12 09 22.79	41 19 41.4	393	0.87	17.2	1.10	0.53	1.43	...	H97,L97

TABLE 2—Continued

RGB J Name	Alternate Name	RA (J2000)	Dec	S_5^{core} (mJy)	F_X ($10^{-12} \frac{\text{erg}}{\text{s cm}^2}$)	O (mag)	α_x	α_{ro}	α_{ox}	z	Ref.
1215+075 ^d	1ES 1212+078	12 15 10.9	07 32 04	84	4.39	17.8	0.88	0.45	1.06	0.130	PG95,B97,L97
1217+301	1ES 1215+303	12 17 52.08	30 07 00.6	353	38.4	15.4	1.88	0.38	1.29	0.237	B95,L96,L97
1220+345	RX J12201+3431	12 20 08.32	34 31 21.6	258	0.42	18.6	0.98	0.61	1.32	...	B95,L96,L97
1221+301 ^d	1ES 1218+304	12 21 21.94	30 10 37.1	60	21.6	16.7	1.22	0.34	1.04	0.182 ^e	B95,L96,L97
1221+282	W COMAE	12 21 31.69	28 13 58.5	940	2.25	15.8 ^a	1.24	0.50	1.51	0.102	B95,L96,K92
1224+246 ^d	MS 1221.8+2452	12 24 24.2	24 36 24	25	2.38	16.9	1.47	0.28	1.40	0.218	B95,P96,L97
1230+253	RX J12302+2517	12 30 14.07	25 18 07.0	351	3.35	17.4	1.89	0.54	1.40	...	N96,B94,L97
1310+323	AU CVn	13 10 28.66	32 20 43.8	1970	0.69	19.9	0.95	0.83	1.06	0.996	B95,U96,G93
1341+399 ^{b,d}	RX J13410+3959	13 41 05.13	39 59 45.5	34	7.92	18.2	...	0.41	0.97	0.163	N96,L97
1417+257 ^d	EXO 1415.6+2557	14 17 56.6	25 43 25	40	23.7	17.5	1.19	0.36	0.90	0.237	B95,L98,L96,L97
1422+580	1ES 1421+582	14 22 38.90	58 01 55.5	6	22.0	18.7	1.04	0.27	0.71	0.638	B95,B94,L97,B98
1427+238	PG 1424+240	14 27 00.39	23 48 00.0	250	6.66	16.4	1.48	0.43	1.32	...	B95,K96,L97
1439+395	PG 1437+398	14 39 17.49	39 32 42.9	38	15.3	18.1	1.55	0.41	0.97	...	B95,L98,F93,L97
1442+120 ^d	1ES 1440+122	14 42 48.3	12 00 40	45	11.0	17.4	1.20	0.37	1.04	0.162	B95,L98,L97
1448+361	RX J14479+3608	14 48 00.58	36 08 31.7	29	6.83	17.2	1.60	0.32	1.23	...	L98,B97,L97
1454+514 ^b	RX J14544+5124	14 54 27.12	51 24 33.6	80	0.95	18.4	...	0.49	1.27	...	L98,L97
1509+559	RX J15098+5555	15 09 47.96	55 56 17.4	28	1.08	18.4	1.99	0.41	1.46	...	K96,B97,L97
1534+372 ^b	RX J15347+3716	15 34 47.20	37 15 54.8	20	0.49	18.3	1.84	0.37	1.55	0.143	L98,B97,L97
1536+016 ^d	MS 1534.2+0148	15 36 46.8	01 37 59	35	8.17	19.9	0.89	0.53	0.67	0.312	B95,P96,L97
1540+147	4C+14.60	15 40 49.49	14 47 45.9	716	1.90	16.4	0.66	0.50	1.36	0.605	B95,U96,L97
1544+049 ^d	RX J15442+0458	15 44 18.7	04 58 22	39	1.70	19.4	0.74	0.51	0.95	...	K96,B97,L97
1555+111	1ES 1553+113	15 55 43.05	11 11 24.4	398	38.7	15.5 ^a	1.45	0.39	1.16	0.360	B95,K96,L97
1602+308	RX J16022+3050	16 02 18.09	30 51 09.3	20	2.11	18.5 ^a	1.56	0.38	1.22	...	L98,K96,L97
1621+377	4C+37.46	16 21 11.29	37 46 04.9	155	1.23	21.4	...	0.78	0.81	...	K96,L97
1624+374	B3 1622+375	16 24 43.35	37 26 42.4	14	0.25	19.4	...	0.42	1.33	0.200	K96,L97

TABLE 2—Continued

RGB J Name	Alternate Name	RA (J2000)	Dec	S_5^{core} (mJy)	F_X ($10^{-12} \frac{\text{erg}}{\text{s cm}^2}$)	O (mag)	α_x	α_{ro}	α_{ox}	z	Ref.
1626+352	RX J16264+3513	16 26 25.85	35 13 41.5	14	1.16	18.7	0.89	0.35	1.14	0.500	K96,K96,L97
1644+457	B3 1642+458	16 44 19.98	45 46 44.5	64	2.60	18.3	1.14	0.46	1.12	0.220	N96,K96,L97,B98
1719+177	PKS J1719+1745	17 19 13.05	17 45 06.4	600	0.87	19.2	...	0.73	1.17	...	B95,VLA
1725+118	1H 1720+117	17 25 04.38	11 52 15.5	88	36.2	16.3 ^a	...	0.35	1.01	0.018	B95,L97
1743+195	1ES 1741+196	17 43 57.84	19 35 08.9	157	9.69	17.3 ^a	0.98	0.47	1.03	0.083	PG95,B97,L97
1747+469	B3 1746+470	17 47 26.65	46 58 50.9	548	0.40	21.3	2.08	0.82	1.10	>1.484	V96,L97
1750+470 ^b	B3 1748+470	17 50 05.00	47 00 43.7	10	4.01	19.0 ^c	0.94	0.37	0.91	0.160	L98,B97,L97
1808+468	RX J18079+4648	18 08 01.20	46 49 41.0	41	0.93	18.4	1.70	0.44	1.40	...	L98,L97
1811+442	RX J18118+4416	18 11 53.47	44 16 28.5	6	0.64	18.9 ^a	1.18	0.31	1.26	...	L98,B97,L97
1813+317	EXO 1811.7+3143	18 13 35.21	31 44 17.7	74	0.99	17.9 ^a	...	0.45	1.33	0.117	PG95,L97
1824+568	4C+56.27	18 24 07.07	56 51 01.5	1120	2.76	18.2	0.15	0.67	1.02	0.664	B95,U96,K92
1829+540	RX J18293+5403	18 29 24.29	54 02 59.8	18	2.35	17.6	2.31	0.31	1.55	...	L98,B97,L97
1838+480	RX J18387+4802	18 38 49.17	48 02 34.4	23	2.78	17.6	2.10	0.33	1.46	...	L98,L97
1841+591	RX J18412+5906	18 41 20.31	59 06 08.2	6	0.74	19.7 ^c	2.54	0.35	1.44	0.530	L98,B97,L97
1848+427	RX J18487+4245	18 48 47.14	42 45 39.4	8	12.2	18.9	1.20	0.34	0.81	...	L98,L97
2039+523 ^b	1ES 2037+521	20 39 23.50	52 19 49.9	19	4.06	19.5 ^a	1.80	0.46	1.05	...	PG95,B97,L97
2145+073	MS 2143.4+0704	21 45 52.30	07 19 27.2	37	8.00	19.0 ^c	1.91	0.47	1.04	0.237	B95,L98,P96,L97
2202+422	BL LACERTAE	22 02 43.29	42 16 40.0	2308	5.68	15.1 ^a	0.94	0.53	1.41	0.0686	B95,U96,L97
2250+384 ^b	B3 2247+381	22 50 05.77	38 24 37.3	60	7.36	16.0 ^{a,c}	1.51	0.29	1.37	0.119	L98,B97,L97
2322+346 ^b	RX J23226+3436	23 22 44.01	34 36 14.0	30	2.83	18.2 ^c	0.80	0.40	1.05	0.098	L98,B97,L97

The Complete Sample

0710+591	1H 0658+595	07 10 30.07	59 08 20.5	34	25.2	18.0 ^c	1.10	0.39	0.81	0.125	PG95,L98,B97,L97
0721+713	1H 0717+714	07 21 53.45	71 20 36.4	600	3.68	15.4	2.02	0.43	1.70	...	B95,B97,VLA
0806+595	RX J08063+5931	08 06 25.94	59 31 06.9	29	4.26	17.2	0.50	0.32	1.09	...	L98,B97,L97
0958+655	S4 0954+65	09 58 47.24	65 33 54.8	480	1.10	16.7	0.24	0.50	1.35	0.367	B95,U96,G93

TABLE 2—Continued

RGB J Name	Alternate Name	RA (J2000)	Dec	S_5^{core} (mJy)	F_X ($10^{-12} \frac{\text{erg}}{\text{s cm}^2}$)	O (mag)	α_x	α_{ro}	α_{ox}	z	Ref.
1031+508	1ES 1028+511	10 31 18.52	50 53 35.8	23	59.2	16.3	1.37	0.21	0.96	0.361	B95,L98,B97,L97,B98
1037+571	RX J10377+5711	10 37 44.31	57 11 55.8	89	2.58	17.4	1.80	0.43	1.41	...	N96,L98,B97,L97
1136+701	MKN 180	11 36 26.41	70 09 27.3	139	58.3	15.5 ^a	1.51	0.32	1.13	0.046	B95,L96,L97
1136+676	RX J11365+6737	11 36 30.08	67 37 04.4	40	24.8	17.4	1.29	0.36	0.93	0.136	L98,B94,L97,B98
1151+589	8C 1148+592	11 51 24.68	58 59 17.6	95	1.66	17.8	0.62	0.46	1.16	...	N96,B97,L97
1231+642	MS 1229.2+6430	12 31 31.40	64 14 18.4	34	4.33	17.0	0.99	0.31	1.19	0.170	B95,P96,L97
1248+583	PG 1246+586	12 48 18.78	58 20 28.7	204	3.25	15.4	1.42	0.34	1.55	...	B95,L97,B98
1415+485	RX J14155+4830	14 15 36.82	48 30 30.5	58	0.44	17.6	1.40	0.40	1.55	...	L98,B97,L97
1419+543	S4 1418+54	14 19 46.60	54 23 14.8	1400	1.22	15.0	1.12	0.47	1.69	0.151	B95,U96,VLA
1427+541 ^b	RX J14274+5409	14 27 30.33	54 09 23.5	24	0.80	17.4 ^c	0.86	0.32	1.37	0.105	L98,B97,L97
1428+426	1H 1430+423	14 28 32.62	42 40 21.1	21	61.4	16.9 ^c	1.05	0.27	0.81	0.130	B95,L98,L96,L97
1516+293 ^b	RX J15166+2917	15 16 41.59	29 18 09.5	34	1.94	18.2 ^c	1.32	0.41	1.22	0.130	L98,B97,L97
1517+654B	1H 1515+660	15 17 47.58	65 25 23.3	19	18.8	17.4	1.16	0.26	0.94	>0.70	PG95,L98,B97,L97,B99
1532+302 ^b	RX J15319+3016	15 32 02.24	30 16 29.0	47	5.87	15.5 ^c	1.00	0.23	1.36	0.064	L98,L97
1533+342	RX J15333+3416	15 33 24.25	34 16 40.2	33	5.49	17.9	1.60	0.38	1.17	...	L98,B97,L97
1542+614	RX J15428+6129	15 42 56.94	61 29 55.3	102	1.46	17.2	1.50	0.42	1.44	...	L98,B97,L97
1554+201	MS 1552.1+2020	15 54 24.13	20 11 25.4	20	5.53	17.5	0.79	0.30	1.05	0.222	B95,P96,L97
1652+403	RX J16527+4023	16 52 49.93	40 23 09.9	11	0.49	17.3	1.80	0.24	1.68	...	L98,L97
1653+397	MKN 501	16 53 52.22	39 45 36.6	450	72.8	14.2	1.35	0.32	1.24	0.033	B95,U96,G93
1704+716	RX J17047+7138	17 04 46.98	71 38 17.6	17	4.28	16.5	2.10	0.22	1.55	...	N96,L98,L97
1728+502	1H 1727+502	17 28 18.62	50 13 10.5	168	31.3	15.2	1.39	0.32	1.24	0.055	B95,L96,L97
1742+597	RX J17424+5945	17 42 32.00	59 45 06.8	77	0.64	17.4	1.96	0.41	1.67	...	L98,B97,L97
1745+398	B3 1743+398B	17 45 37.76	39 51 30.8	118	1.59	18.3 ^c	...	0.51	1.20	0.267	L98,L97
1748+700	S5 1749+70	17 48 32.84	70 05 50.8	610	2.14	16.9	1.77	0.51	1.45	0.770	B95,U96,K92
1749+433	B3 1747+433	17 49 00.36	43 21 51.3	281	0.47	17.9	1.32	0.56	1.47	...	V96,L97

TABLE 2—Continued

RGB J Name	Alternate Name	RA (J2000)	Dec	S_{5}^{core} (mJy)	F_X ($10^{-12} \frac{\text{erg}}{\text{s cm}^2}$)	O (mag)	α_x	α_{ro}	α_{ox}	z	Ref.
1756+553	RX J17561+5522	17 56 15.89	55 22 18.1	10	13.6	17.9	1.64	0.28	1.04	...	L98,B97,L97
1806+698	3C 371	18 06 50.68	69 49 28.1	950	2.51	14.9 ^a	1.28	0.44	1.64	0.0512	B95,U96,G93
2243+203	RX J22438+2020	22 43 54.73	20 21 03.9	86	0.97	16.0	1.68	0.31	1.72	...	L98,B97,L97
2319+161	RX J23196+1611	23 19 43.44	16 11 50.1	17	3.23	17.9 ^a	1.20	0.32	1.15	...	L98,B97,L97

^aOptical magnitude converted from another band to equivalent O mag ($\alpha_{\text{opt}}=1.0$); See notes below

^bID Uncertain; see notes below

^cOptical magnitude corrected to include AGN component only

^dFrom low radio resolution sample

^eNew redshift from Perlman, Schachter & Stocke (1998)

^fRedshift of 0.135 reported in Nass et al. 1996 is incorrect (Bade, private communication)

References to Table 2:

B94: Bade et al., 1994

B95: Brinkmann et al., 1995

B97: Brinkmann et al., 1997

B98: Bade et al., 1998

B99: Beckmann, 1999

F93: Fleming et al., 1993

F98: Fischer et al., 1998

G93: Ghisellini et al., 1993

H97: Henstock et al., 1997

K92: Kollgaard et al., 1992

K96: Kock et al., 1996

L96: Lamer et al., 1996

L97: Laurent-Muehleisen et al., 1997

L98: Laurent-Muehleisen et al., 1998

M96: Marchā et al. 1996

N96: Nass et al., 1996

P96: Perlman et al., 1996b

PG95: Padovani & Giommi, 1995

R99: Rector, Stocke & Perlman, 1999

U96: Urry et al., 1996

V96: Vermeulen et al., 1996

VLA: VLA Calibrator List

Notes to individual sources in Table 2:

0007+472: Optical position given in Kock et al. (1996) is $2.1''$ from radio position; $V=18.3$ mag

0040+408: Padovani & Giommi (1995) report object as candidate

0110+418: $Br_{4000}=32\%$; $O(\text{Total})=17.3$ mag

0115+253: ID based on 80 \AA resolution spectrum

0152+017: $Br_{4000}=29\%$; $O(\text{Total})=16.1$ mag

0153+712: Marchā et al. (1996) report $P=3\%$, $Br_{4000}=33\%$ and $W_{\lambda}([\text{H}\alpha, \text{[NII]})=17\text{ \AA}$; $E(\text{Total})=15.5$ mag

0202+088: ID based on 80 \AA resolution spectrum

0214+517: Marchā et al. (1996) report $P=2\%$ and $Br_{4000}=15\%$ and $W_{\lambda}<3\text{ \AA}$; $E(\text{Total})=16.5$ mag

0227+020: ID based on 80 \AA resolution spectrum

0314+247: $W_{\lambda}([\text{OII}]\lambda 3727)=14\text{ \AA}$; $W_{\lambda}([\text{OIII}]\lambda 5007)=12\text{ \AA}$; $Br_{4000}=30\%$; $O(\text{Total})=17.3$ mag

0450+450: The X-ray emission in the vicinity of this source is highly complex and it is unclear how much (if any) of the X-ray emission is actually associated with the BL Lac; $V=18.5$ mag

0650+250: $V=15.3$ mag

0654+427: Marchā et al. (1996) report $P=2-3\%$, $Br_{4000}=17\%$ and $W_{\lambda}(\text{H}\alpha, \text{[NII]})=8\text{ AA}$; $O(\text{Total})=17.6$ mag

0656+426: $Br_{4000}=36\%$; Star-forming Elliptical?; $O(\text{Total})=15.1$ mag

0710+591: $Br_{4000}=22\%$; $O(\text{Total})=17.4$ mag

0916+526: ID based on 80 \AA resolution spectrum

0929+502: ID based on 80 \AA resolution spectrum

0930+350: Henstock et al. (1997) report source is weak, but no emission lines observed

1000+225A: Optical counterpart between two radio sources; Upper limit reported to core radio flux

1012+424: Optical spectrum contains unidentified emission lines with $W_{\lambda}=10\text{ \AA}$ & 4 \AA

1047+546: Padovani & Giommi (1995) report object as candidate

1053+494: Rector, Stocke & Perlman (1999) report $W_{\lambda}(\text{H}\alpha)=2.5\text{ \AA}$ & $Br_{4000}=32\%$; $O(\text{Total})=16.4$ mag

1136+701: $V=15.0$ mag

1341+399: ID based on 80 \AA resolution spectrum

1427+541: $Br_{4000}=39\%$; $O(\text{Total})=15.8$ mag

1428+426: $Br_{4000}=1\%$; $O(\text{Total})=16.9$ mag

1454+514: Flat Fielding error at $\sim 8380\text{ AA}$?

1516+293: $Br_{4000}=32\%$; Star-forming Elliptical?; $O(\text{Total})=17.1$ mag

1532+302: $Br_{4000}=29\%$; $O(\text{Total})=14.6$ mag

1534+372: $W_{\lambda}([\text{H}\alpha, \text{[NII]})=4\text{ \AA}$; Br_{4000} not measured

1555+111: $V=15.0$ mag

1602+308: $E=17.5$ mag

1621+377: Strongest line in spectrum in Kock et al. (1996) is $W_{\lambda}=9 \text{ \AA}$
1725+118: $V=15.8 \text{ mag}$
1743+195: $V=16.8 \text{ mag}$
1745+398: $Br_{4000}=17\%$; $O(\text{Total})=17.8 \text{ mag}$
1750+470: $Br_{4000}=29\%$; $O(\text{Total})=18.1 \text{ mag}$
1806+698: $V=14.4 \text{ mag}$
1813+317: $V=17.4 \text{ mag}$
1841+591: $Br_{4000}=17\%$; $O(\text{Total})=19.2 \text{ mag}$
2039+523: Padovani & Giommi (1995) report object as candidate
2145+073: $Br_{4000}=10\%$; $O(\text{Total})=18.8 \text{ mag}$
2250+384: $Br_{4000}=7\%$; Star-forming Elliptical?; $E(\text{Total})=14.8 \text{ mag}$
2319+161: $E=17.0 \text{ mag}$
2322+346: $Br_{4000}=33\%$; Star-forming Elliptical?; Uncorrected $O(\text{Total})=17.0 \text{ mag}$